NASA Contractor Report 182079
ICASE Report No. 90–50

ICASE

AN INVESTIGATION OF CHAOTIC KOLMOGOROV FLOWS

N. Platt
L. Sirovich
N. Fitzmaurice

Contract No. NAS1–18605
August 1990

Institute for Computer Applications in Science and Engineering
NASA Langley Research Center
Hampton, Virginia 23665–5225

Operated by the Universities Space Research Association

National Aeronautics and
Space Administration

Langley Research Center
Hampton, Virginia 23665-5225

AN INVESTIGATION OF CHAOTIC KOLMOGOROV FLOWS

N. Platt
Center for Fluid Dynamics and Division of Applied Mathematics
Brown University

L. Sirovich[1]
Center for Fluid Mechanics and Division of Applied Mathematics
Brown University

N. Fitzmaurice[1]
Department of Mathematics
Case Western University

ABSTRACT

A two-dimensional flow governed by the incompressible Navier-Stokes equations with a steady spatially periodic forcing (known as the Kolmogorov flow) is numerically simulated. The behavior of the flow and its transition states as the Reynolds number Re varies is investigated in detail, as well as a number of the flow features. A sequence of bifurcations is shown to take place in the flow as Re varied. Two main regimes of the flow have been observed: small and large scale structure regimes corresponding to different ranges of Re. Each of the regimes includes a number of quasiperiodic, chaotic and relaminarization windows. In addition, each range contains a chaotic window with non-ergodic chaotic attractors. Spatially disordered, but temporally steady states have been discovered in large scale structure regime. Features of the diverse cases are displayed in terms of the temporal power spectrum, Poincare sections and, where possible, Lyapunov exponents and Kaplan-Yorke dimension.

[1]Research was supported by the National Aeronautics and Space Administration under NASA Contract No. NAS1-18605 while the authors were in residence at the Institute for Computer Applications in Science and Engineering (ICASE), NASA Langley Research Center, Hampton, VA 23665.

1 Introduction

It is now well established that a number of dissipative chaotic fluid flows may require relatively few dimensions for their description[1-4]. This has been examined perhaps in greatest detail for fluid models such as the Ginzburg-Landau (G-L) equation[5-8], an equation which results from the study of the critical point in a variety of stability problems[9-12]. For closed fluid systems such as Rayleigh-Bénard (R-B) convection and Taylor-Couette flow there is abundant evidence that the early stages of chaos are low dimensional. For R-B convection there also exists a numerical simulation which details the variation of dimension with Rayleigh number[13].

In this paper we consider a simple fluid flow which exhibits chaotic behavior and which is amenable to detailed examination. This flow, governed by the incompressible Navier-Stokes equations, is generated and maintained by a spatially periodic time independent forcing of the fluid. It is sometimes referred to as the Kolmogorov flow (Arnold and Meshalkin[14]). The stability of the primary flow has been reported on by Meshalkin and Sinai[15] and Green[16]. That flow is known to become unstable at a critical Reynolds number, Re_c, of $\sqrt{2}$ [15,16], beyond which a stationary cellular pattern appears[17]. At sufficiently high Re the cellular pattern itself becomes unstable and the resulting flow is unsteady and chaotic. Kraichnan[18] and Batchelor[19] have shown that two

dimensional turbulent flows exhibit an energy cascade toward low wavenumbers (the infamous reverse cascade) and an enstrophy cascade toward high wavenumbers. This phenomenon is apparent in our calculations. An alternate view of this effect, in the present instance, is that the flow is unstable to long wavelength disturbances. The general instability of short wavelength structures to long wavelength disturbances has been investigated by Yakhot and Sivaskinsky, and under sufficiently anisotropic conditions, their study lead to the notion of negative viscosity for the long wavelengths[20,21], since the growth rate is proportional to the square of the wavenumber.

Our investigation is in large part numerical in nature. We examine in some detail the behavior of the flow and its transition states for a range of the bifurcation parameter Re. We use Poincare sections to examine the chaotic attractor of the flow, and apply the Kaplan-Yorke formula[22] to calculate the dimension of the chaotic attractor when it is possible. A number of remarkable features of the flow were discovered. These include windows of relaminarization in the parameter space, chaotic windows with *non-ergodic* attractors and spatially disordered but temporally steady states.

We will be careful throughout this paper to use the term *chaotic* instead of the term *turbulent*. In particular we are referring to flows which when looked at in the time domain have broad band energy spectra. These flows also exhibit sensitive dependence on initial data (they have positive Lyapunov

exponents). Thus by generally accepted criteria the flows are temporally chaotic. However, as will be seen, relatively few spatial Fourier modes are active and we say we have chaos rather than turbulence. Nevertheless the flow is chaotic in its Eulerian description and should not be confused with *Lagrangian turbulence*[23–25] in which the velocity fields are to a high degree laminar.

Recently we became aware of the investigation of the Kolmogorov Flow by She[26,27]. While there is some unavoidable overlap, the two investigations are largely complimentary. She's work is also mainly numerical and concentrates on the high end of the Re range. (A minor difference is that he uses a higher value for the frequency of the forcing function.) The mathematical tools used also differ. We will make extensive use of the power spectra, Poincare sections, Lyapunov spectra and flow visualizations for the investigation, while She relies mainly on time series and phase portraits. Several issues are viewed differently by us and we comment on these in the text. She's further work done in collaboration with Nicolaenko is concentrated on the symmetry breaking homoclinic chaos[28,29] occurring beyond the Re range covered in this study.

2 Kolmogorov Flow

We consider the forced incompressible Navier-Stokes equations in two dimensions,

$$\partial'_x u' + \partial'_y v' = \nabla' \cdot \mathbf{u}' = 0 \tag{2.1}$$

$$\frac{d}{dt'}\mathbf{u}' + \nabla p'/\rho = \nu \nabla'^2 \mathbf{u}' + \chi \sin ky' \mathbf{e}_x \tag{2.2}$$

In preparation for the normalization given below, dimensional quantities are denoted by primes, $\mathbf{e}_x$ denotes the unit vector in the x-direction. This system has the solution or *fixed point*,

$$\mathbf{u}' = \mathbf{U}' = \frac{\chi \mathbf{e}_x}{k^2 \nu} \sin ky'. \tag{2.3}$$

A Reynolds number for the flow may be naturally based on the maximum speed of this field, $\chi/\nu k^2$ and the length scale k^{-1}, thus

$$Re = \chi/(k^3 \nu^2). \tag{2.4}$$

(A Reynolds could be based on the wavelength and maximum speed in which case $2\pi Re$ is the Reynolds number).

The linear stability of (2.3) can be analyzed by writing

$$\mathbf{u}' = \mathbf{U}' + \delta \mathbf{u}'(y) \exp(i\alpha kx + \sigma t) \tag{2.5}$$

and investigating the resulting Orr-Sommerfeld equation gotten by linearization in the small perturbation, $\delta \mathbf{u}'$[30]. It is found that instability first sets in

at[15,16]

$$Re = Re_c = \sqrt{2} \tag{2.6}$$

and is due to disturbances of infinitely long wavelength. Moreover, it can be shown that disturbances with $\alpha k > 1$ never destabilize U'.

Thus according to the stability analysis, the domain must be large in some sense in order for us to include growing modes. For computational purposes we fix the domain size and regard the spatial forcing frequency as the bifurcation parameter. With this in mind we choose the following normalization,

$$\mathbf{u} = \nu k^2 \mathbf{u}'/\chi,\ \mathbf{x} = k\mathbf{x}'/n,\ t = \chi t'/(nk\nu), p = p'\nu^2 k^4/\chi^2, \tag{2.7}$$

where n is an integer which specifies the spatial frequency of the forcing. Under this normalization the Navier-Stokes equations become,

$$\nabla \cdot \mathbf{u} = 0 \tag{2.8}$$

$$\frac{d\mathbf{u}}{dt} + \nabla p = \frac{1}{\Omega} \nabla^2 \mathbf{u} + \frac{n^2}{\Omega} \mathbf{e}_x \sin ny \tag{2.9}$$

with

$$\Omega = n\chi/(\nu^2 k^3) = nRe \tag{2.10}$$

the bifurcation parameter. In this format the critical value of Ω is

$$\Omega_c = nRe_c = n\sqrt{2}. \tag{2.11}$$

Let us now briefly discuss the symmetry groups for the solutions of these equations which we will refer to as the Kolmogorov flows[31]. There are in fact two groups, one discrete and the other continuous.

Referring back to the notation of (2.9), n refers to the number of vertical cycles in the horizontal forcing. If $[u(x,y,t), v(x,y,t)] = \mathbf{u}$ is a solution then

$$g^k\mathbf{u} = [(-)^k u\left((-)^k x, y + k\frac{\pi}{n}\right), v\left((-)^k x, y + k\frac{\pi}{n}\right)] \; k = 0, \ldots, 2n-1, \tag{2.12}$$

are also (independent) solutions of the problem, i.e. they satisfy the equations and conditions of the problem. The generator of this cyclic group, g, is a *glide-reflection*[32] of half wavelength. In addition rotation through π is another group generator, i.e.

$$R\mathbf{u} = [-u(-x,-y), -v(-x,-y)] \tag{2.13}$$

is also a solution. In all there are $4n$ elements in the discrete symmetry group for the Kolmogorov flow. Thus for the case being considered, $n = 4$, we obtain a sixteen-fold increase in the number of possible solutions which we can view.

The remaining symmetry group is the group of translations in the x-directions, i.e. if $\mathbf{u}$ is a solution then

$$T_l\mathbf{u} = [u(x+l, y), v(x+l, y)] \tag{2.14}$$

are also solutions to the problem for all $0 \leq l \leq 2\pi$.

3 Computational Method

Based on the normalization given in the previous chapter we consider the computational domain

$$0 \leq x, y \leq 2\pi \tag{3.1}$$

with periodic boundary conditions in the two directions (so the flow lies on the torus).

The natural method of choice for the investigation of (2.8,9) under the 2π-periodic boundary conditions is the pseudo-spectral method using Fourier expansions[33]. All derivatives are evaluated in the spectral space and updates are performed on the expansion coefficients of $\mathbf{u}(\mathbf{x}, t)$. On the other hand the non-linear terms are evaluated in the physical space and then transformed back to the spectral space. The needed transformations are all efficiently done by the means of the Fast Fourier Transforms.

In a variation on the usual formulation we have used the vector expansion set

$$\mathbf{B}_{\mathbf{m}}(\mathbf{x}) = \frac{(m_2, -m_1)}{\mid \mathbf{m} \mid} \exp(i\mathbf{m} \cdot \mathbf{x}), \tag{3.2}$$

where $\mathbf{m}$ is the integer wavenumber pair (m_1, m_2). Using such a basis we can expand the velocity field $\mathbf{u}$ as

$$\mathbf{u}(\mathbf{x}, t) = \sum_{\mathbf{m}} u_{\mathbf{m}}(t) \mathbf{B}_{\mathbf{m}}(\mathbf{x}) \tag{3.3}$$

where the sum is performed over all the components of the wave vector $\mathbf{m}$.

The basis elements are easily seen to be divergence free,

$$\nabla \cdot \mathbf{B_m} = 0 \tag{3.4}$$

and complete in the space of square integrable 2π-periodic divergence-free vector functions. An advantage of this formulation is that gradients of scalar functions (such as the pressure term in the Navier-Stokes equations) are orthogonal to the divergence-free space[34] and so a result of a Galerkin formulation is that pressure is eliminated entirely from the problem. A computational method of this type was used be Leonard and Wray[35] in their study of the stability of pipe flows.

Throughout our study the underlying forcing frequency was taken to be n=4 and so that the critical value of the bifurcation parameter Ω is

$$\Omega_c = 4\sqrt{2}. \tag{3.5}$$

Furthermore, we shall be interested in the long-term, asymptotic behavior of the flows developing from the primary flow

$$\mathbf{u} = \mathbf{U} = \frac{\sin 4y}{\Omega}\mathbf{e}_x, \tag{3.6}$$

which is a fixed point solution of (2.8,9). To facilitate this study we use a small fixed perturbation of the primary flow including all positive and negative wavenumbers as the initial conditions for the calculations. In particular,

we set

$$\mathbf{u}_o(\mathbf{x},0) = \frac{1}{\Omega}\sin 4y\mathbf{e}_x + \frac{10^{-4}}{2\Omega}\sum_{\substack{m_1\geq 0\\ m_2\geq 0}}[(1+i)\mathbf{B}_{\mathbf{m}}(\mathbf{x}) - (1-i)\mathbf{B}_{-\mathbf{m}}(\mathbf{x})] \quad (3.7)$$

If we write

$$\mathbf{u}_o = (u_o, v_o) \quad (3.8)$$

then for example u_o has the form

$$u_o = \frac{1}{\Omega}\left(\sin 4y + 10^{-4}\sum_{\substack{m_1\geq 0\\ m_2\geq 0}}\frac{m_2}{|\,\mathbf{m}\,|}(\cos(m_1x+m_2y) - \sin(m_1x+m_2y)\right) \quad (3.9)$$

The computations were performed for the range

$$\Omega/\Omega_c \leq 12.5 \quad (3.10)$$

After allowing a considerable time for the calculation to settle down (on average 5000 time units), we examine the resulting flow on the attractor. It was found out that a 32×32 spatial grid was adequate for the resolution at the ratios (3.10). Two types of dealiasing were used during the course of the simulation as were grids of twice the resolution. Neither were found to significantly alter the results.

4 Tools of the Analysis

Here we briefly comment on the tools used in the analysis of the direct numerical simulation of the Kolmogorov flow. The tools needed for the investigation can be grouped according to their function.

4.1 Temporal Power Spectra

We need some mathematical tools to distinguish between chaotic and quasiperiodic regimes of the flow. The temporal power spectra (PS) are indispensable for this purpose[36].

Let $PS(\gamma(t))$ denote the temporal PS of the time signal $\gamma(t)$. It follows from equation (3.3) that there are $32^2 = 1024$ individual time histories available for the use in the temporal PS. For the problem at hand, we define the energy PS box averaged per m_1 wavenumber in x-direction as (modulo a multiplicative normalization)

$$PS(\mathbf{u})^{(m_1)} = \sum_{m_2} PS(Re(u_{(m_1,m_2)}(t))) + PS(Im(u_{(m_1,m_2)}(t))). \qquad (4.1)$$

In other words, we take the temporal PS of all the time histories resulting from the projections onto basis function (3.2) which include m_1 in the wavenumber pair $\mathbf{m} = (m_1, m_2)$ and average over them. This is in keeping with the definition of the PS of a time stationary signal as being the Fourier transform of the autocorrelation. In the calculations we frequently set m_1 to

zero and use the resulting temporal power spectrum to distinguish between chaotic and quasiperiodic regimes of the flow.

For later reference we remark now that since the PS is the Fourier transform of the autocorrelation it follows that as the frequency $| f | \rightarrow \infty$ the PS vanishes faster than any inverse power of $| f |$. This is a simple consequence of the fact that in any numerical simulation we are integrating a system of ordinary differential equations with smooth direction fields and hence the solution is C^{∞} in the time variable.

4.2 Poincare Sections

We use Poincare sections to study geometrical structure of the attractor and to qualitatively discuss its degree of complication. Methods for the calculation of these sections have been given by Keefe[5] and others. The phase space employed in the calculation of the Poincare sections is spanned by the spatial Fourier modes of the solution $\mathbf{u}(\mathbf{x}, t)$

$$\mathbf{u}(\mathbf{x}, t) = \sum_{\mathbf{m}} u_{\mathbf{m}}(t) \mathbf{B}_{\mathbf{m}}(\mathbf{x}) \tag{4.2}$$

where $\mathbf{u}_{\mathbf{m}}$ and $\mathbf{B}_{\mathbf{m}}$ are complex.

The choice of the sectioning plane for the Kolmogorov flow becomes very important, for it determines which attractor features are covered by the study. Here, we are mainly concern with the visual structure of the attractor itself. CPU expenditures to accumulate a large enough collection of

points for a highly resolved Poincare section become considerable. Therefore a need arises for the use of the discrete symmetry group of the flow to extend the available data. This in turn suggests that some care should be exercised in the choice of a sectioning plane. In particular, an acceptable choice is a plane which is invariant under the symmetry group. It is also a good practice to choose as a section, a plane for which the flow projections maximize the energy. With that in mind, we take the forcing function plane

$$Im(u_{(0,4)}) = D \tag{4.3}$$

$$Im(\dot{u}_{(0,4)}) > 0 \tag{4.4}$$

as our invariant under the action of the symmetry group section plane for the Poincare sections used later. The choice of the constant D controls apparent positioning of the hyperplane in the phase space and is dependent upon Ω. In actual calculations, we consider a series $[Im(u_{(0,4)}(t_i))]_{i=1}^{N}$ of snapshots of the variable $Im(u_{(0,4)}(t))$. We then set D to its average, i.e.

$$D = \frac{1}{N}\sum_{i=1}^{N} Im(u_{(0,4)}(t_i)). \tag{4.5}$$

The Poincare sections shown in the later sections plot $Re(u_{(0,1)})$ vs $Im(u_{(0,1)})$.

For further reference, we note here representation of the symmetry group (2.12,13) in terms of the spectral components of $\mathbf{u}(\mathbf{x},t)$. If $\mathbf{u}(\mathbf{x},t)$ is represented as in (4.2) then the glide-reflection $g\mathbf{u}(\mathbf{x},t)$ (2.12) can be written as

$$g\mathbf{u}(\mathbf{x},t) = \sum_{\mathbf{m}} -u_{(-m_1,m_2)}(t)e^{i\frac{m_2}{n}\pi}\mathbf{B_m}(\mathbf{x}) = \sum_{\mathbf{m}} u^*_{(m_1,-m_2)}(t)e^{i\frac{m_2}{n}\pi}\mathbf{B_m}(\mathbf{x}) \tag{4.6}$$

while the rotation Ru (2.13) is

$$R\mathbf{u}(\mathbf{x},t) = \sum_{\mathbf{m}} u_{-\mathbf{m}}(t)\mathbf{B_m}(\mathbf{x}) = \sum_{\mathbf{m}} -u^*_{\mathbf{m}}(t)\mathbf{B_m}(\mathbf{x}) \tag{4.7}$$

It then follows from (4.5) and (4.6-7) that our sectioning plane is invariant under the symmetry group of the flow.

From the examination of the equation (4.7), it is apparent that the rotation corresponds to the reflection around imaginary axis for any variable $u_{\mathbf{m}}(t)$. On the other hand glide-reflection action (4.6) of the symmetry group on $u_{(0,1)}(t)$ gives

$$-u_{(0,1)}(t)e^{i\frac{\pi}{4}} \tag{4.8}$$

This corresponds to $\frac{5}{4}\pi$ rotation in $Re(u_{(0,1)}(t)) - Im(u_{(0,1)}(t))$ plane. Thus the discrete symmetry group of the flow induces an extra symmetries onto $u_{(0,1)}(t)$ plane. They correspond to the reflection around $\frac{1+2i}{8}\pi$, $i = 0,1,2,3$ axis. These symmetries figure prominently in the discussion of the results of our numerical simulation.

4.3 Lyapunov Spectrum

All of the mathematical tools mentioned above can indicate the presence of chaos in the dynamical system, but do not directly address the level of randomness present, or how chaotic a solution is.

We compute the Lyapunov exponents for the two dimensional Navier-Stokes equations (2.8,9) to study the dimension of the attracting set of the chaotic flow. We write the governing system in symbolic form as

$$\frac{d\mathbf{u}}{dt} = \mathcal{F}(\mathbf{u}), \tag{4.9}$$

and denote a reference or fiducial trajectory by $\mathbf{u}^o$. If an initially nearby trajectories is written as

$$\mathbf{u} = \mathbf{u}^o + \epsilon \mathbf{v} \tag{4.10}$$

then in the limit $\epsilon \to 0$, $\mathbf{v}$ satisfies the variational equation,

$$\frac{d}{dt}\mathbf{v} = \mathcal{L}(\mathbf{u}^o)\mathbf{v} \tag{4.11}$$

where

$$\mathcal{L}(\mathbf{u}^o) = \frac{\delta \mathcal{F}(\mathbf{u}^o)}{\delta \mathbf{u}^o} \tag{4.12}$$

is easily obtained through the linearization.

The largest Lyapunov exponent is defined as the maximum exponential rate at which nearby trajectories diverge

$$\lambda_1 = \lim_{\tau \to \infty} \frac{1}{\tau} \ln \|\mathbf{v}(\tau)\| \tag{4.13}$$

Thus the idea of a Lyapunov exponent can be regarded as a generalization of the stability exponent of an equilibrium solution, and finding a positive Lyapunov exponent is an unambiguous signature of a chaos.

In a practical sense we expect all initial data, $\mathbf{v}(0)$, to lead to λ_1, i.e., as time evolves $\mathbf{v}$ will become parallel to the direction of greatest growth. Thus to obtain the next greatest growth rate, and so forth can be a touchy problem. Algorithms for calculating these has been given by Bennetin et al[37], Shimeda and Nagashima[38] and Wolf et al[39], and are further explained by Fitzmaurice[40]. The essence of the trick lies in computing volumes of infinitesimal ellipsoids. In fact if $\epsilon_n(\tau)$ denotes the volume of an n-ellipsoid it then follows that

$$\lambda_1 + \lambda_2 + \ldots + \lambda_n = \lim_{\tau \to \infty} \frac{1}{\tau} \ln \epsilon_n(\tau). \tag{4.14}$$

Thus after (4.13) one calculates $\lambda_1 + \lambda_2$, then $\lambda_1 + \lambda_2 + \lambda_3$, etc and thereby the spectrum $\lambda_1, \lambda_2, \ldots$.

Since the system in question is dissipative we know that the sum (4.14) will become negative for n large enough. And since it is chaotic it must be positive for $n = 1$. Therefore this sum must cross zero at some point as one increases n. One may then use the formula of Kaplan and Yorke[22]

$$d_L = N - \frac{\sum_k \lambda_k}{\lambda_{N+1}} \tag{4.15}$$

to estimate the dimension, d_L, of the attractor where N is the largest integer for which the sum is positive. Constantin et al[41] have shown that the Kaplan-Yorke formula gives an upper bound for the Hausdorf dimension.

5 Results

In this section we present the results of our direct numerical simulation of the Kolmogorov flow. We have found that there are two main regimes of the flow corresponding to different ranges of the bifurcation parameter Ω. Tentatively these are termed as being the regimes of small and large scale structures. Explanation for this terminology will be evident from the streamline plots to be discussed.

5.1 Small Scale Structures

$0 < \Omega/\Omega_c \leq 1$

For this range the asymptotic solution of the N-S equations (2.8,9) is the fixed point (3.6). Streamlines and vorticity plots for the parallel shear flow in horizontal direction are shown in Figure 1.

$1 < \Omega/\Omega_c < 1.97$

As we increase Ω, the horizontal shear flow becomes unstable and the flow pattern changes. At $\Omega/\Omega_c = 1$, the parallel shear flow bifurcates to a new solution. In this range the motion is steady and purely cellular and illustrations of this are shown in Figures 2 and 3. It is interesting to note that at the lower range of the parameter Ω the flow is almost horizontal (Figure

2a) while at higher values of Ω in this range the motion is mainly in the vertical direction (Figure 3a) with well defined cells. In the first instance the saddle points of the separatrices are formed horizontally while in the latter case they are joined vertically. This is in an agreement with the experiments of Bondarenko, et al[42] for a magnetohydrodynamic problem under similar forcing.

$1.97 \leq \Omega/\Omega_c \leq 2.22$

In this range the flow still have the steady cellular structure but the number of cells in the horizontal direction have doubled. The new flow patterns are depicted in Figure 4. Explanation of this phenomena relies on the fact that the horizontal wavenumber of the fastest growing mode changes from 1 to 2, also reported by Green[16]. A very important feature of the flow in this and previous ranges is that it is invariant under the discrete symmetry group transformations. By invariance we mean that for any transformation G in the discrete symmetry group of the flow there is $0 \leq l \leq 2\pi$ such that

$$T_l G\mathbf{u} = \mathbf{u} \tag{5.1}$$

where T_l is a translation by l in x-direction and $\mathbf{u}$ is a solution of N-S equations (2.8,9). In words, we say that the flow is invariant under the discrete symmetry group if, after application of any transformation from the discrete

symmetry group to the flow, we can translate the transformed flow in horizontal direction in such a way that it coincides with the original flow.

$2.2 < \Omega/\Omega_c < 3.53$

As Ω increases, small amplitude perturbations at the saddle points will lead to the destabilization and eventual breakdown of the steady cellular pattern. At $\Omega/\Omega_c = 2.2$ another bifurcation in parameter space takes place. For the range under discussion there is a gradual breakdown in the symmetry of the flow. The new flow patterns are depicted in Figure 5. It is perhaps remarkable that these cellular structures are still steady.

$3.53 \leq \Omega/\Omega_c \leq 3.6$

At $\Omega/\Omega_c = 3.53$ the statistically stationary flow is no longer steady. Now, the flow spends most of the time in the steady cellular state shown in Figure 5. But from time to time, the flow is intermittently disturbed by a random horizontal shifts occuring on a very rapid time scale. The time between bursts is very long and is a decreasing function as the parameter Ω reaches the upper end of the range. Figure 6 shows the time series of $Re(u_{(0,1)})$. Here, the plateaus correspond to a steady cellular state. After the horizontal shift, the cells oscillate with a small amplitude for a short while,

and then settle down very rapidly to a steady pattern before undergoing the next horizontal shift. This state is chaotic but only over a very long time scale, i.e. the Lyapunov spectrum has some very small positive exponent.

$3.6 < \Omega/\Omega_c < 4.47$

In this range the nature of the flow changes once again. We now find a periodic oscillations occuring in the cellular structures as depicted in Figure 5. Also, the solution develops a slow drift in horizontal direction, but without a net transport off mass. The drift may be regarded as the wave motion. It also follows from symmetry that the drift wave can move in either direction. We conclude from Figure 7 which shows the temporal power spectrum that there is a principal frequency, the large peak, and subharmonic frequencies of it present in the flow. These correspond to the oscillations of the pattern around larger vortices and inner oscillations of the vortices themselves. It is interesting to note that we have found no regime of the flow when only the principal frequency is present.

$4.47 \leq \Omega/\Omega_c < 4.58$

Now, the flow enters its second chaotic regime. Figure 8 depicts a typical time series of the signal $Re(u_{(0,1)})$ in this range, from which we con-

clude that the chaos is intermittent. Examining the power spectrum shown in Figure 9, we see that the principal and subharmonic frequencies are prominently present in what is a broad band spectrum. We did not attempt to calculate the Kaplan-Yorke dimension for the dynamical system in this range of Ω because of the very long time interval between the bursts of activity in the flow. A most remarkable feature of the flow in this range is that the chaotic attractor is *not ergodic*! The dynamical system has several chaotic attractors each with its own basin of attraction lying quite close to the fixed point (3.6). On the basis of extremely long calculations we conclude that these attractors are not connected. Figure 10 shows the Poincare section depicting cuts of the chaotic attractors. Two darker points in the blown up section Figure 10b correspond to the punctures produced by the solution in the laminar phase of the intermittency. In actual calculations we obtain only one of the attractors (depending on the chosen initial data) , and the rest are obtained by using the discrete symmetry group. Alternatively, we can apply the symmetry group to the initial data and thus generate each of the attractors. Another peculiarity of the flow is that there are only eight symmetric attractors instead of sixteen as predicted by the discrete symmetry group. This happens because the action of five glide-reflections followed by the rotation by π applied to the solution maps the attractor onto itself. This induces an extra symmetry into the attractor corresponding to the reflection

around the axis denoted by the dashed line in Figure 10b, as it is discussed in the earlier part of this paper dealing with the Poincare sections.

$4.58 \leq \Omega/\Omega_c \leq 4.65$

As Ω increase, different symmetric attractors start intersecting each other and now the flow is intermittenly chaotic with one ergodic attractor consisting of eight connected symmetric components. Figure 11 shows the time series of $Re(u_{(0,1)})$. The evidence of the intermittent bursts is clearly present and sudden jumps correspond to the solution jumping to a different component of the attractor. We present the temporal power spectrum in Figure 12. This new state is more chaotic than the previous case, but still there is evidence of the principal frequency from the lower parameter values. The Poincare section is shown in Figure 13 ("butterflies" section). Darker regions in the blown up section of the attractor in Figure 13b correspond to the points where the solution spends most of the time between intermittent bursts. Moreover, comparing Figures 13 and 10, we notice that the main features of the non-ergodic attractor are still present.

$4.65 < \Omega/\Omega_c \leq 4.71$

Another remarkable feature of the Kolmogorov flow is, that counter

to intuition, the parameter space Ω contains windows of relaminarization between different chaotic ranges of the flow. This range is an example of one of such windows. Here, the flow returns to a periodic regime with a principal and subharmonic frequencies in the power spectrum. Again, there is no regime with just one frequency. This flow is similar to the range $3.6 < \Omega/\Omega_c < 4.47$. It also, develops a slow steady drift in the horizontal direction. We also note that this drift appears to vanish in the chaotic windows of the flow.

At $\Omega = 4.72\Omega_c$ we see the formation of large scale structures.

5.2 Large Scale Structures

Although we are mainly interested in the asymptotic behavior of the Kolmogorov flow, it is of interest to examine how the large scale structures are formed. The process is basically the same for all values $\Omega \geq 4.72\Omega_c$.

We start with a small perturbation of the fixed point flow (3.6). This state persists for roughly the time scale predicted by the linear stability analysis. Then on a very rapid time scale the flow changes to the unsteady cellular pattern of the sort illustrated in Figure 5. This state with many small cells persists for a very short time and then the flow plunges into chaos. The new state is vigorously chaotic, characterized by the rapid movements of a small vortical structures, a snapshot of which is shown in Figure 14. By a rough

count it is seen that the same number of vortical structures appears in Figure 5 and 14. We refer to this state as *metastable* or *transient* chaos following the terminology of Grebogi, Ott and Yorke[43]. Of all the chaotic states observed in our numerical experiments, this is the only state which can be called chaotic both spatially and temporally and hence is turbulent according to common convention. At the lower range of Ω this *metastable* chaos holds for a relatively long time, while at a higher values of the bifurcation parameter Ω it can be extremely short.

In any case the phase point finds an escape hole in the metastable attractor and we eventually see the formation of a large scale structures such as those depicted in the Figure 15. The new attractor is stable. Considerable vortex merging has taken place in passing from Figure 14 to Figure 15. The two large structures shown in the streamline plot of Figure 15a are somewhat misleading. On a closer examination of the vorticity plot, we see that we have roughly the same number of distinct vortices as before and that the large structures in the streamline plot consist of a number of a counterrotating vortices. These new large scale structures are completely different from the small scale structures which we dealt in the previous subsection. Examining the vorticity plot shown in Figure 5b, we notice that at the small scales the vortices arranged in a lattice. Thus, the unsteady small scale structures flow can be considered as oscillations or "breathing" of the lattice structure.

In the *metastable* regime this lattice structure is broken, and we have a soup of vortices moving randomly around. Later the vortices merge together and arrange themselves on a curved line with two vortices containing most of the circulation. These vortices correspond to the eyes of the large scale structures depicted in the streamline plot of Figure 15a. It is of interest to note here that the vertical position of the eyes of the large scale structures are at hyperbolic points of the forcing functions when the flow is not chaotic.

We will now describe in detail the bifurcations occuring in the large scale structure regime of the flow.

$4.72 \leq \Omega/\Omega_c < 5.9$

In this range the flow is periodic with one frequency. In addition, there is a horizontal drift present in the solution as also noted by She[26]. As Ω/Ω_c approaches 5.9 both the frequency of oscillations and drift speed approach zero. Figure 16 shows the temporal power spectrum.

$\Omega = 5.9\Omega_c$

At $\Omega = 5.9\Omega_c$, the flow reaches the steady, spatially disorganized state depicted in Figure 15. The flow is chaotic only in the spatial domain!

$5.9 < \Omega/\Omega_c < 9.47$

As we start increasing Ω further, the flow develops both periodic oscillations and a slow drift in the horizontal direction. The direction of the drift changes according to the particular attractor the flow settles in. Moreover, as Ω increases, so does the drift speed and frequency of the oscillations. The periodic oscillations can be described as the "breathing" in the inner shells of the large scale structures. At $\Omega = 9.042\Omega_c$ a period doubling bifurcation takes place in the oscillations of the inner structures. Now the principal and subharmonic frequencies correspond to the breathing of the large scale structure itself and the oscillations of the inner shells. This regime persists up to $\Omega = 9.45\Omega_c$, where another period doubling bifurcation in the oscillations takes place. We can see clearly the principal and subharmonic frequences in Figure 17 showing the temporal power spectrum of the flow.

$9.47 \leq \Omega/\Omega_c < 9.66$

At $\Omega = 9.47\Omega_c$ the flow enters another chaotic regime which continues until Ω reaches $9.66\Omega_c$. We again find the remarkable feature in this window that there is chaos but that the attractors are *non-ergodic*! Here, the chaos is present in the irregular breathing-like oscillations of the inner structures which induces random oscillations of large scale structures. We observe

in Figure 18, which shows the temporal power spectrum, that the driving frequency and its subharmonics still dominate the motion. Horizontal drift diminishes to a trickle and sometimes changes directions. On average, there is no drift at all. Figure 19 depicts the Poincare section of the attractor showing eight symmetric disconnected attractors. The slopes of the lines in Figure 20 correspond to the values of Lyapunov exponents and the calculated Kaplan-Yorke dimension is 7.9.

$9.66 \leq \Omega/\Omega_c < 10.805$

At $\Omega = 9.66\Omega_c$ the flow enters another laminar window in the parameter space Ω. Here, the solution slowly drifts in the horizontal direction and has the principal and subharmonic frequencies. At $\Omega/\Omega_c = 10.4$ a period doubling bifurcation takes place. Figure 21 shows the temporal power spectrum at $\Omega = 10.7\Omega_c$.

$10.805 \leq \Omega/\Omega_c \leq 12.5$

As we increase Ω even further, the flow enters another chaotic regime at $\Omega = 10.805\Omega_c$. The flow now appears to be governed by an ergodic attractor which consists of eight symmetrical components and the solution intermittently jumps from one component to another. There is a very long time

delay between successive jumps at Ω slightly greater than the 10.805, but it rapidly decreases as Ω increases. The driving frequency and its subharmonics dominate the power spectrum shown in Figure 22. An examination of Figure 23 showing the Poincare section of the chaotic attractor, indicates that the components of the attractor have a fractal structure. The calculated Kaplan-Yorke dimension is 8.9. Another interesting point is that the direction of the drift changes with each successive jump to a different component of the attractor.

As we continue to increase Ω, the different components of the chaotic attractor merge together and become indistinguishable. Nevertheless, the driving and subharmonic frequencies are still dominate the temporal power spectrum shown in Figure 24 for $\Omega = 12.5\Omega_c$. Now, the Kaplan-Yorke dimension increases to 10.8. Thus we might hope to describe the system in terms of a dynamical system having many fewer than roughly 1000 degrees of freedom that we have been allowing in our spectral simulations.

As in the case of the small scale structures, the average drift speed diminishes to zero for the chaotic regimes and the drift is not present at all for $\Omega \geq 12.5\Omega_c$.

This concludes our detailed description of the behavior of the fixed point (3.6) of the Kolmogorov flow as a function of the bifurcation parameter Ω.

6 Summary

In this paper we investigated in some detail a simple fluid flow governed by the incompressible two-dimensional Navier-Stokes equations with a spatially periodic time independent forcing. Two main regimes of the flow have been observed: small and large scale structure regimes corresponding to different ranges of Reynolds number Re. A sequence of bifurcations takes place in each of the regimes of the flow.

The first three bifurcations taking place in the small scale structure regime are steady: the first corresponds to the appearance of the cellular structures, the second doubles the horizontal wavenumber of the cellular structures, while the third breaks the symmetry of the flow. In addition, three chaotic windows are discovered in the small scale structures regime. The first window is chaotic over a very long time scale. The second window is an intermittency with a remarkable feature that the chaotic flow has *non-ergodic* attractors. Finally, the last chaotic window shows intermittency with one connected chaotic attractor consisting of eight symmetric components ("butterflies"). There are laminar windows between the first and the second chaotic regimes, and after the last chaotic regime.

The large scale structure regime contains a number of quasi-periodic and chaotic windows. Before the formation of the large scale structures, the flow

spends considerable time in *metastable* chaos which approaches true turbulent flow for the range of Re under the discussion. A spatially disordered, but temporally steady state was observed between first two laminar windows. Two period-doublings take place in the second laminar window. The chaotic regime which follows has the same remarkable property of chaotic but *non-ergodic* attractors as is the case with the small scale structure regime. In addition, there is a window of relaminarization with a quasi-periodic flow between the two chaotic regimes.

In the future, we plan to use the proper-orthogonal decomposition[44] to extract the coherent structures of the flow and study the resulting low order dynamical systems[45].

Acknowledgement: The work was supported by DARPA-URI Grant Number N00014-86-K0754. Numerical simulations were carried out on the NAS facility at the NASA Aimes Research Center and at the Pittsburgh Supercomputer Center.

References

[1] Gollub, J.P. and S.V. Benson, *Many routes to turbulent convection*, Jour. Fluid Mech. (1980).

[2] Brandstater, A., J. Swift, H. Swinney, H.L. Wolf, D. Farmer, E. Jen, and P. Crutchfield, *Low-dimensional chaos in a hydrodynamic system*, Phys. Rev. Lett. **51**, 1442, (1983).

[3] Fenstermacher, P.R., H.L. Swinney and J.P. Gollub, *Dynamical instabilities and the transition to chaotic Taylor vortex flow*, Journ. Flu. Mech. **94**, 103, (1979).

[4] Malraison, B., P. Atten, P. Berge and M. Dubois, *Dimension d'attracteurs étranges: une détermination expérimentale au régime chaotique de deux systéme convectifs*, Comptes-rendu del'Academie des Sciences de Paris, **C297**, 209, (1983).

[5] Keefe, L., *Dynamics of perturbed wavetrain solutions to the Ginzburg-Landau equation*, Stud. Appl. Math., **73**, 91-153, (1985).

[6] Doering, C., J.D. Gibbon, D. Holm and B. Nicolaenko, *Low dimension behavior in the complex Ginzburg-Landau equation*, Contemporary Mathematics, AMS, (1989).

[7] Sirovich, L. and J.D. Rodriguez, *Coherent structures and chaos: A model problem*, Physics Letter A, **120**, No. 5, (1987).

[8] Sirovich, L., J.D. Rodriguez and B. Knight *Two boundary value problems for the Ginzburg-Landau problem*, Physica D **43** (1) (to appear) (June, 1990).

[9] Newell, A.C. and J.A. Whitehead, *Finite bandwidth, finite amplitude convection*, J. Fluid Mech. **38**, 279, (1969).

[10] Newell, A.C., *Envelope equations, in nonlinear wave motion*, A.C. Newell ed., AMS, (1974).

[11] Hocking, L.M., K. Stewartson and J.T. Stuart, *A nonlinear instability burst in plane parallel flow*, J. Fluid Mech., **51**, 705-735, (1972).

[12] Hasimoto, H., and H. Ono, *Nonlinear modulation of gravity waves*, J. Phys. Soc. Japan, **33**, 805, (1972).

[13] Deane, A.E. and L. Sirovich, *Lyapunov spectrum and attractor dimension for chaotic Rayleigh-Bénard convection*, **(to appear in JFM in 1990).**

[14] Arnold, V.I. and L.D. Meshalkin, Uspekhi Mat. Nauk, **15**, 247 (1960).

[15] Meshalkin, L.D. and Ia.G. Sinai, *Investigation of the stability of a stationary solution of a system of equations for the plane movement of an incompressible viscous liquid*, PMM, **25**, 1140-1143, (1961).

[16] Green, J.S.A., *Two dimensional turbulence mear the viscous limit*, Journ. Fluid Mech **62**, pp.273-287, (1974).

[17] Sivaskinsky, G.I., *Weak turbulence in periodic flows*, Physica D **17**, 243-255, (1985).

[18] Kraichnan, R.H., *Inertial ranges in two-dimensional turbulence*, Phys. Fluids, **10**, 1417, (1967).

[19] Batchelor, G.K., *Computation of the energy spectrum in homogeneous two dimensional turbulence*, Phys. Flu. (Suppl. 2) **12**, 233, (1969).

[20] Sivaskinsky, G.I. and V. Yakhot, *Negative viscosity effect in large-scale flow*, Phys. Flu., **28**, 1040-1042, (1985).

[21] Yakhot, V. and G.I. Sivaskinsky, *Negative-viscosity phenomena in three-dimensional flows*, Phys. Rev A, **35**, 815-820, (1987).

[22] Kaplan, J. and J. Yorke, in: *Functional Differential Equations and Approximation of Fixed Points*, (H.O. Peitgen and H.O. Walther, eds.) Springer-Verlag, New York, (1979).

[23] Ottino, J.M, C.W. Leong, H. Rising and P.D. Swanson, *Morphologonal structures produced by mixing in chaotic flows*, Nature **33**, 419-425, (1988).

[24] Aref, H., *Stirring by chaotic advection*,J. Fluid Mech., **143**, 1-21, (1984).

[25] Rom-Kedar, V., A. Leonard and S. Wiggins, *An analytic study of transport mixing and chaos in an unsteady vortical flow* ,JFM, **214**, 347-394, (1990).

[26] She, Z.S., *Large-Scale Dynamics and Transition to Turbulence in the Two-Dimensional Kolmogorov Flow*, Proc. on Current trends in turbulent research, AIAA, 374-396, (1988).

[27] She, Z.S., *Metastability and vortex pairings in the Kolmogorov Flow*, Physics Letters A, **124**, No. 3, 161-164, (1987).

[28] She, Z.S. and B. Nicolaenko, *Temporal intermittency and turbulent production in the Kolmogorov flow*, to appear in IUTAM Symposium, Aug. 1989, Cambridge University Press, (1989).

[29] Nicolaenko, B. and Z.S. She, *Symmetry breaking homoclinic chaos in Kolmogorov flows*, to appear in Proceedings of Kiev Conference, (1989).

[30] Drazin, P.G. and W.H. Reid, *Hydrodynamic Stability*, Cambridge University Press, (1981).

[31] Sirovich, L., *Turbulence and the dynamics of coherent structures, Pt. II: Symmetries and transformations*, Quart. Appl. Math., **45**, 573-582, (1987).

[32] Birkoff, G. and S. MacLane, *Survey of Modern Algebra*, MacMillan, New York, (1941).

[33] Canuto, C., M.Y. Hussaini, A. Quarderonic, and T.A. Zang, *Spectral Methods in Fluid Dynamics*, Springer-Verlag, N.Y., 1987.

[34] Ladyshenskaya, O.A., *The Mathematical Theory of Incompressible Viscous Flow*, Gordon and Breach, N.Y., (1969).

[35] Leonard, A. and A. Wray, *A new numerical method for simulation to three dimensional flow in a pipe*, in: Proc. 8th International Conference on Numerical Methods in Fluid Dynamics, Aachen, ed. E. Krause, Lecture notes in Physics **170**, Springer-Verglag, N.Y., (1982).

[36] Berge, P., Pomeau, Y., C. Vidal, *Order within Chaos*, John Wiley & Sons, Inc., New York, 1986

[37] Bennetin, G.L., A. Galgani, A. Giorgilli and J. Strelayn, *Lyapunov characteristic exponents for smooth dynamical systems and for Hamiltonian systems: A method for computing all of them*, Pts. 1 and 2. Meccanica, **15**, p 9-30, (1980).

[38] Shimada, I. and T. Nagashimi, *A numerical approach to the ergodic problem of dissipative dynamical systems*, Prog. Theor. Phys., **61**, 1605, (1979).

[39] Wolf, A., J.B. Swift, H.L. Swinney and J.A. Vastamo, *Determining Lyapunov exponents from a time series*, Physica **16D**, p 285-317, (1985).

[40] Fitzmaurice (MacGiolla Mhuiris), N., *Lyapunov exponents for infinite dimensional dynamical systems*, Advances in Comp. Methods for P.D.E.'s, **6**, 460, (1987).

[41] Constantin, P., C. Foiaş, O.P. Manley and R. Temam, *Determining modes and fractal dimension of turbulent flows*, J. Fluid Mech. **150**, 427-440, (1985).

[42] Bondarenko, N.F., M.Z. Gak and F.V. Dolzhansky, *Laboratory and Theoretical Models of Plane Periodic Flows*, Atmospheric and Oceanic Physisc **15**, 711-716, (1979).

[43] Grebogi, C., E. Ott and J.A. Yorke, *Chaos Strange Attractors and Fractal Basin Boundaries in Nonlinear Dynamics*, Science, **238**,p. 632-638, (1987).

[44] Sirovich, L., *Turbulence and the dynamics of coherent structures, Pt. I: Coherent structures*, Quart. Appl. Math., **45**, 561-571, (1987).

[45] Sirovich, L., *Turbulence and the dynamics of coherent structures, Pt. III: Dynamics and scaling*, Quart. Appl. Math., **45**, 583-590, (1987).

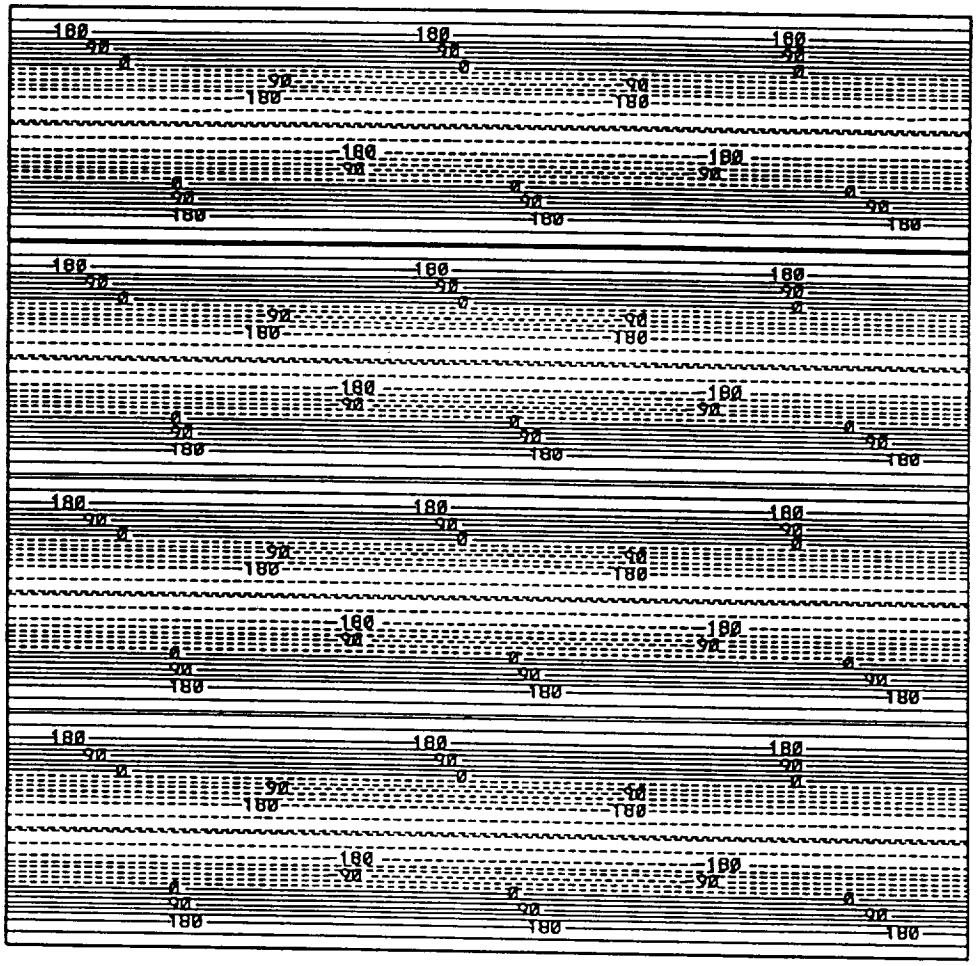

1. Parallel shear layer flow corresponding to the fixed point solution at $\Omega = 0.5\Omega_c$. a) streamlines.

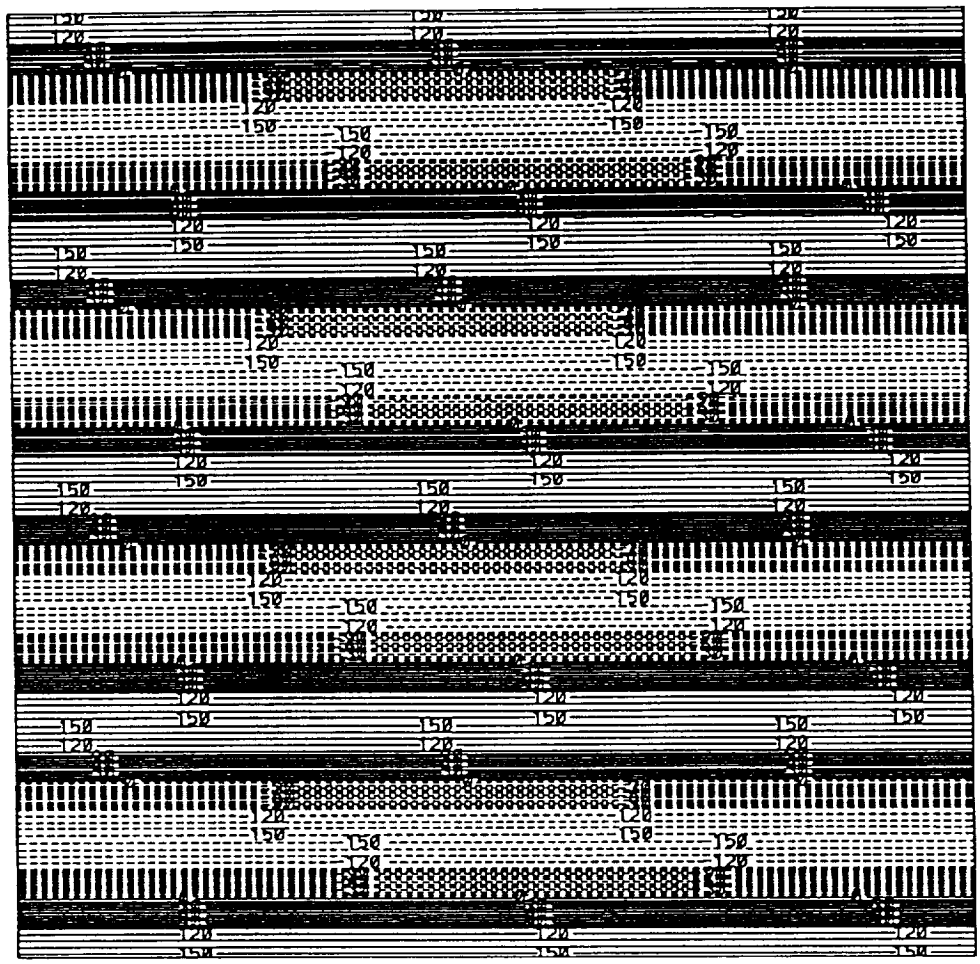

1. Parallel shear layer flow corresponding to the fixed point solution at $\Omega = 0.5\Omega_c$. b) vorticity.

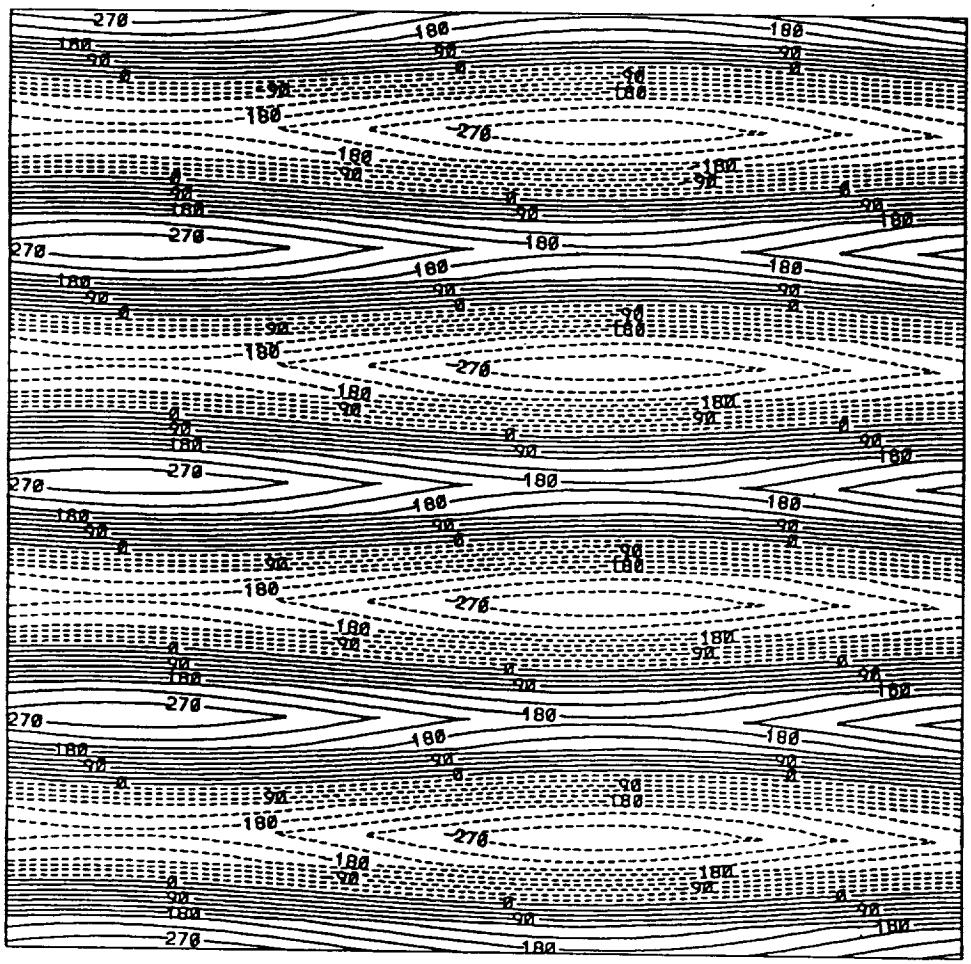

2. Steady cellular flow found at $\Omega = 1.12\Omega_c$ with the motion mainly in horizontal direction. a) streamlines.

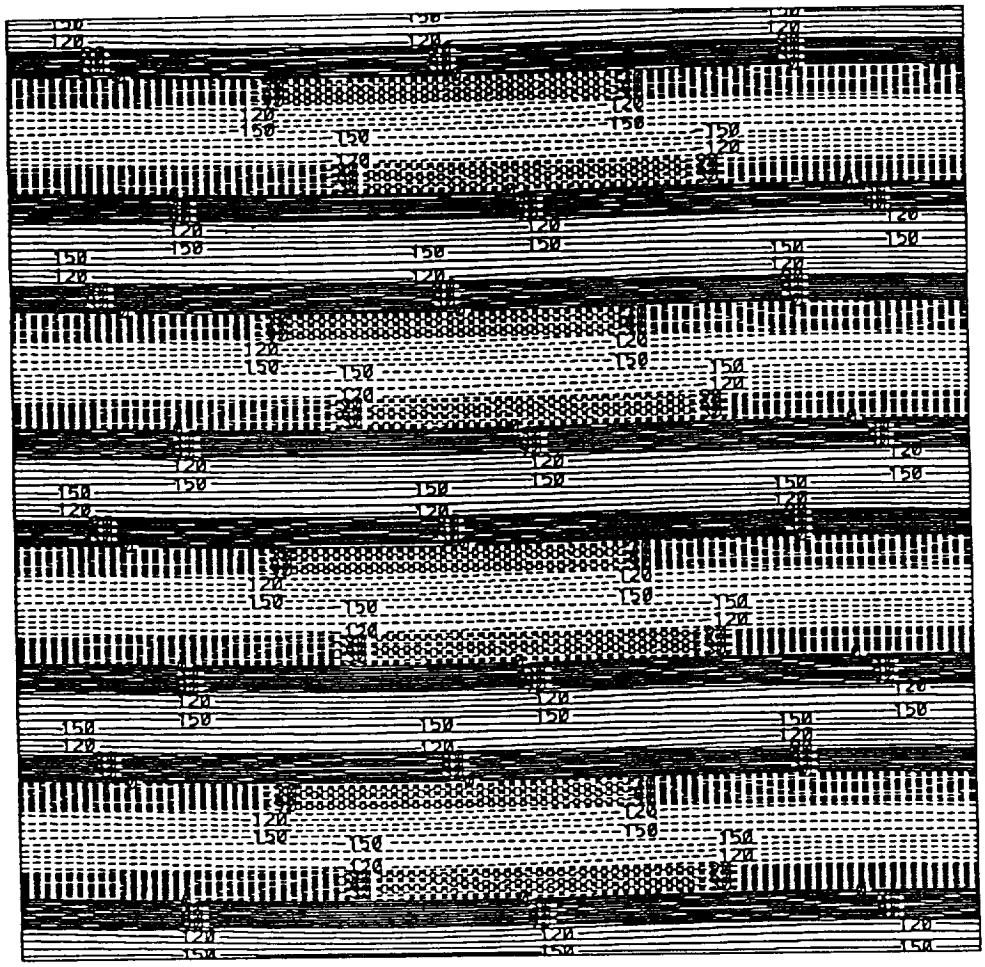

2. Steady cellular flow found at $\Omega = 1.12\Omega_c$ with the motion mainly in horizontal direction. b) vorticity.

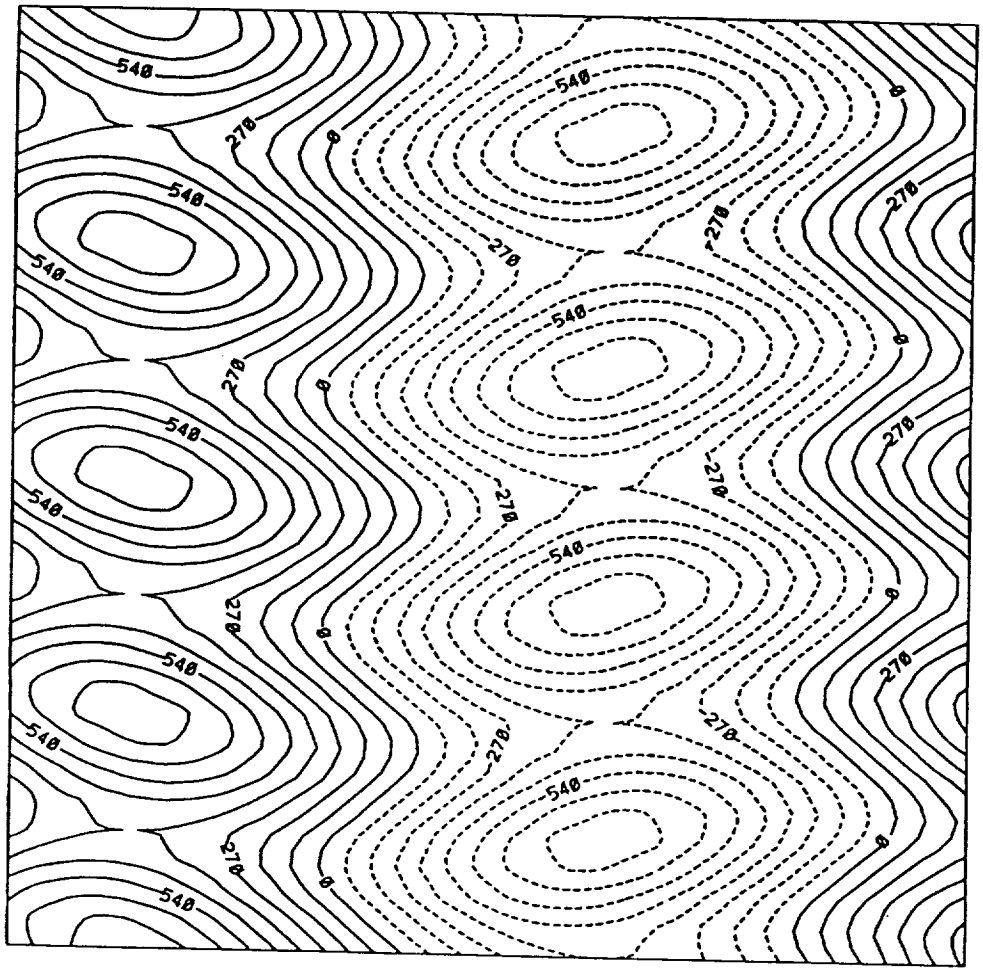

3. Steady cellular flow found at $\Omega = 1.5\Omega_c$ with the motion mainly in vertical direction and the fastest growing perturbation with wavenumber 1 in horizontal direction. a) streamlines.

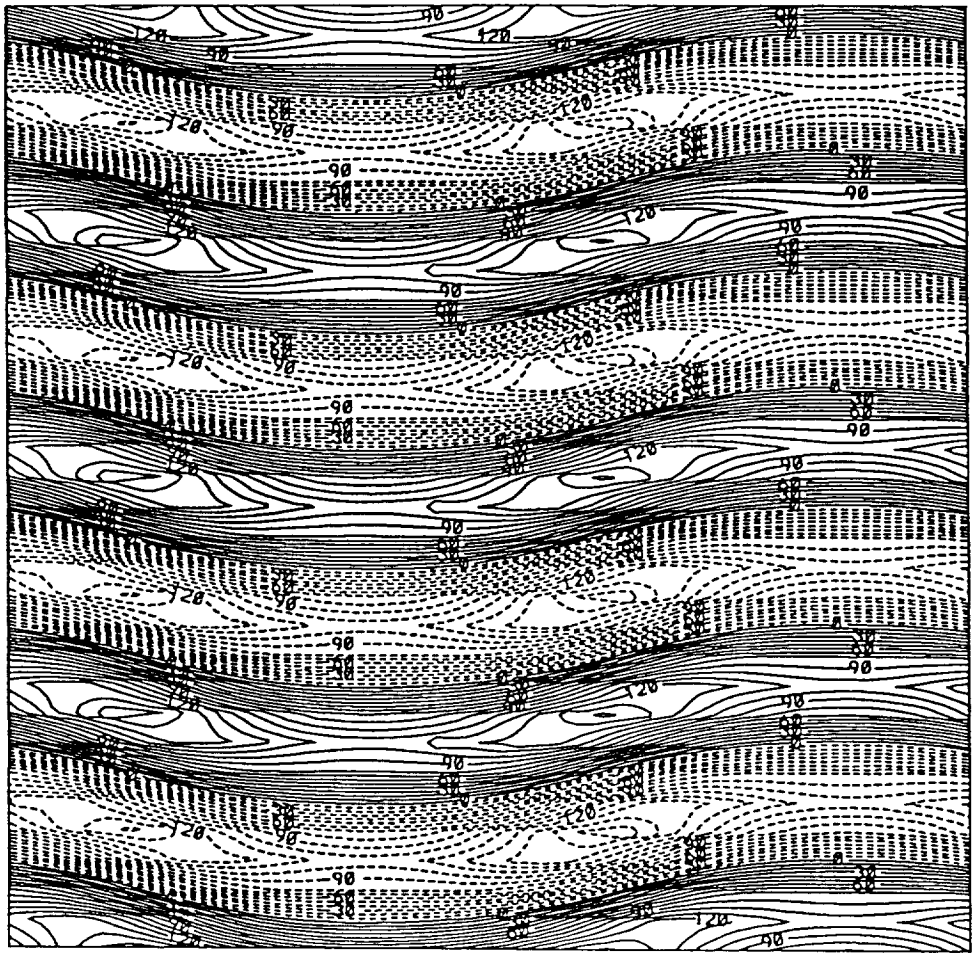

3. Steady cellular flow found at $\Omega = 1.5\Omega_c$ with the motion mainly in vertical direction and the fastest growing perturbation with wavenumber 1 in horizontal direction. b)vorticity.

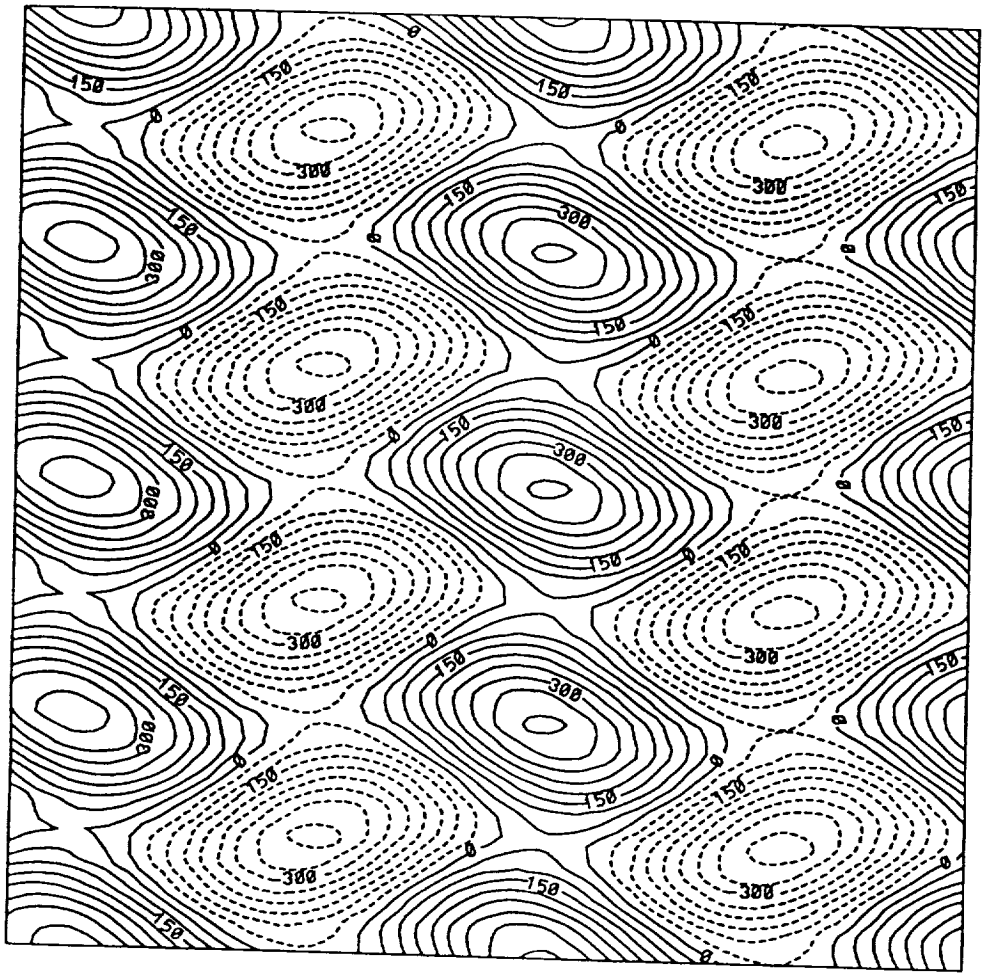

4. Steady cellular flow found at $\Omega = 2\Omega_c$ with the motion mainly in vertical direction and the fastest growing perturbation with wavenumber 2 in horizontal direction. a) streamlines.

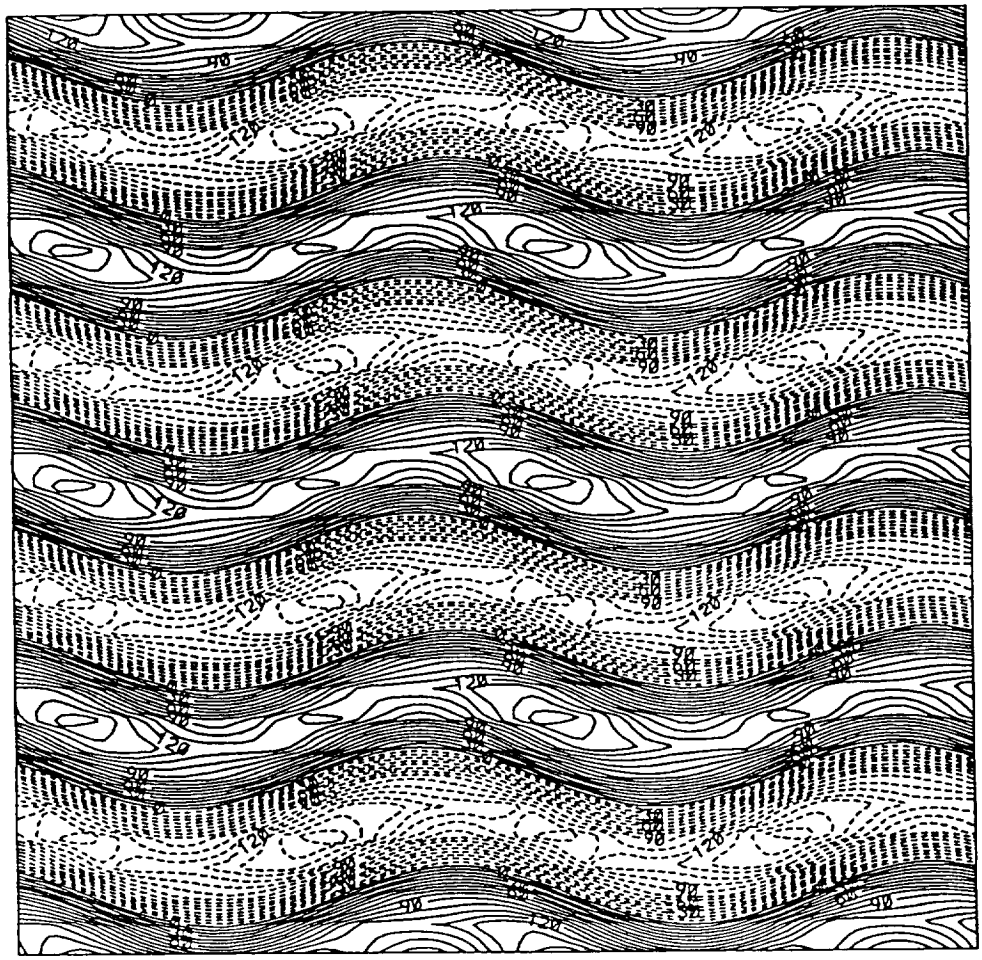

4. Steady cellular flow found at $\Omega = 2\Omega_c$ with the motion mainly in vertical direction and the fastest growing perturbation with wavenumber 2 in horizontal direction. b) vorticity.

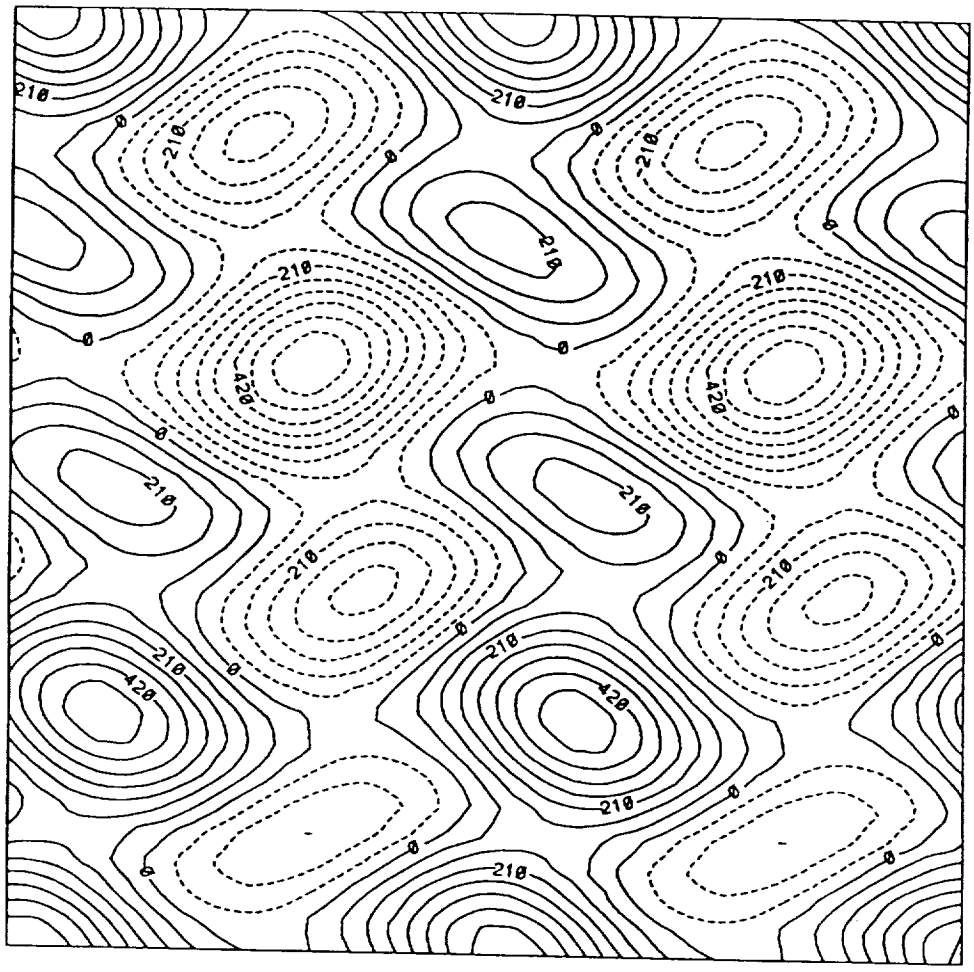

5. Steady cellular flow found at $\Omega = 3\Omega_c$. a) streamlines.

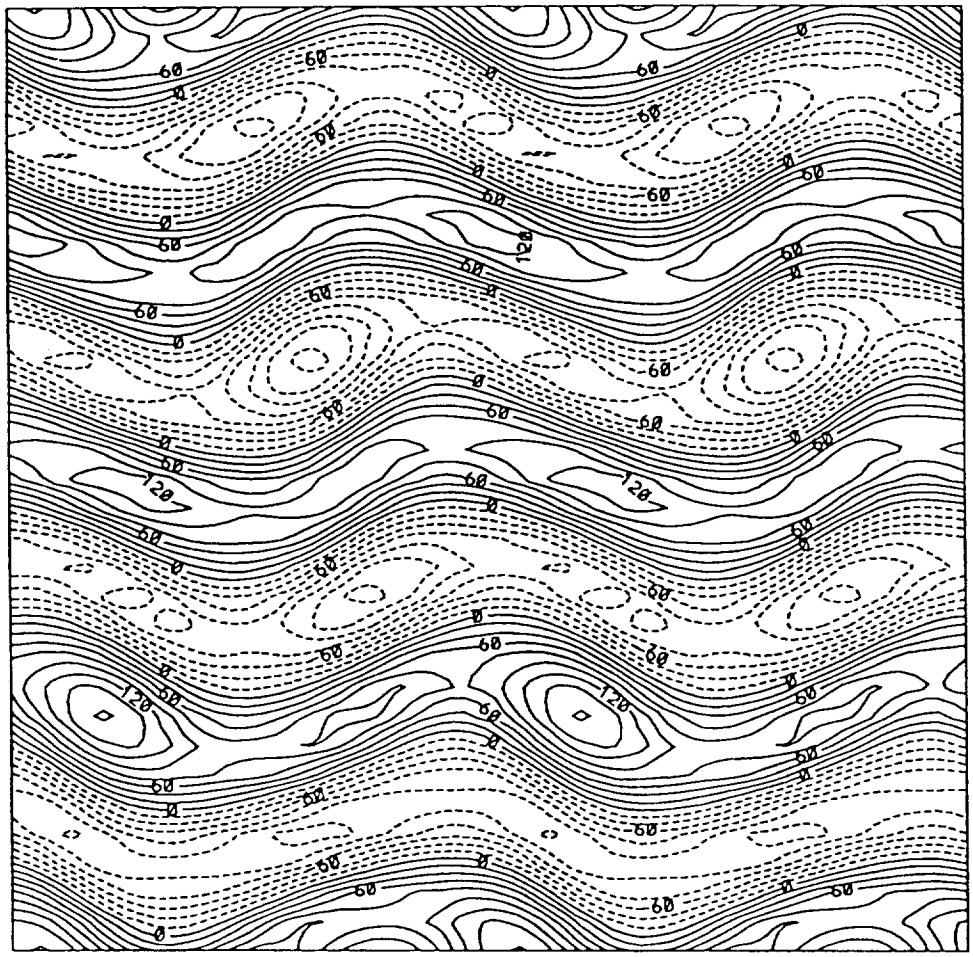

5. Steady cellular flow found at $\Omega = 3\Omega_c$. b) vorticity.

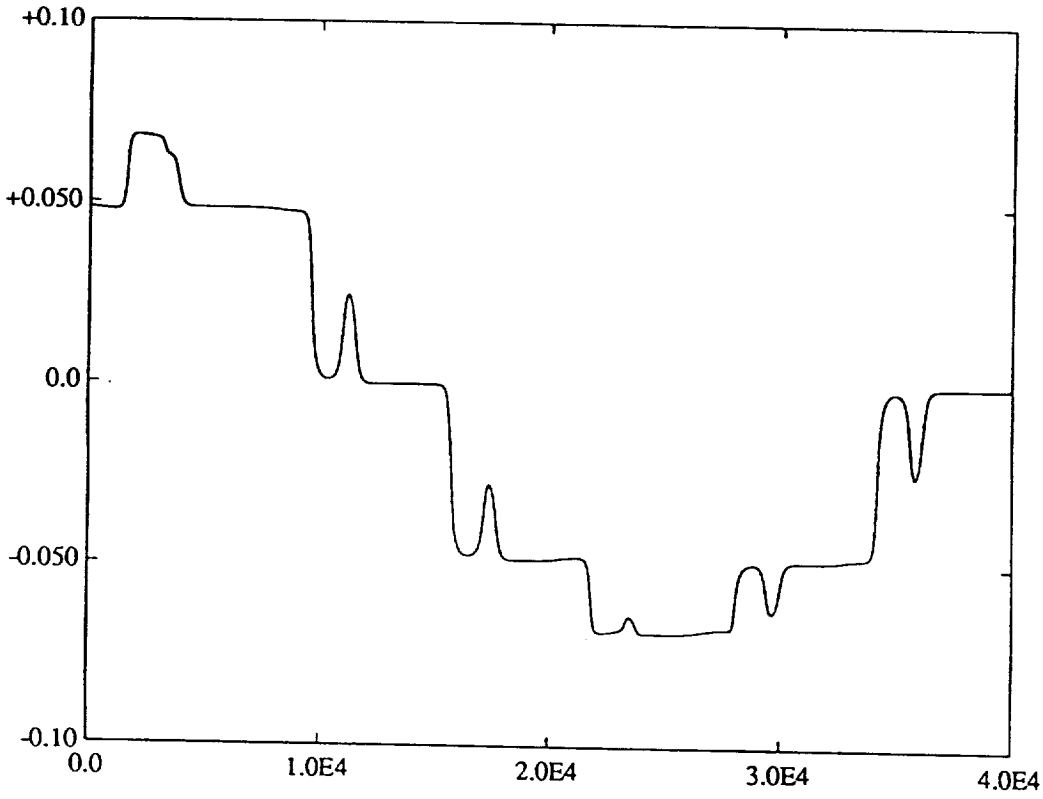

6. Time series of $Re(u_{(0,1)})(t)$ at $\Omega = 3.56\Omega_c$. Plateaus correspond to a steady cellular flow.

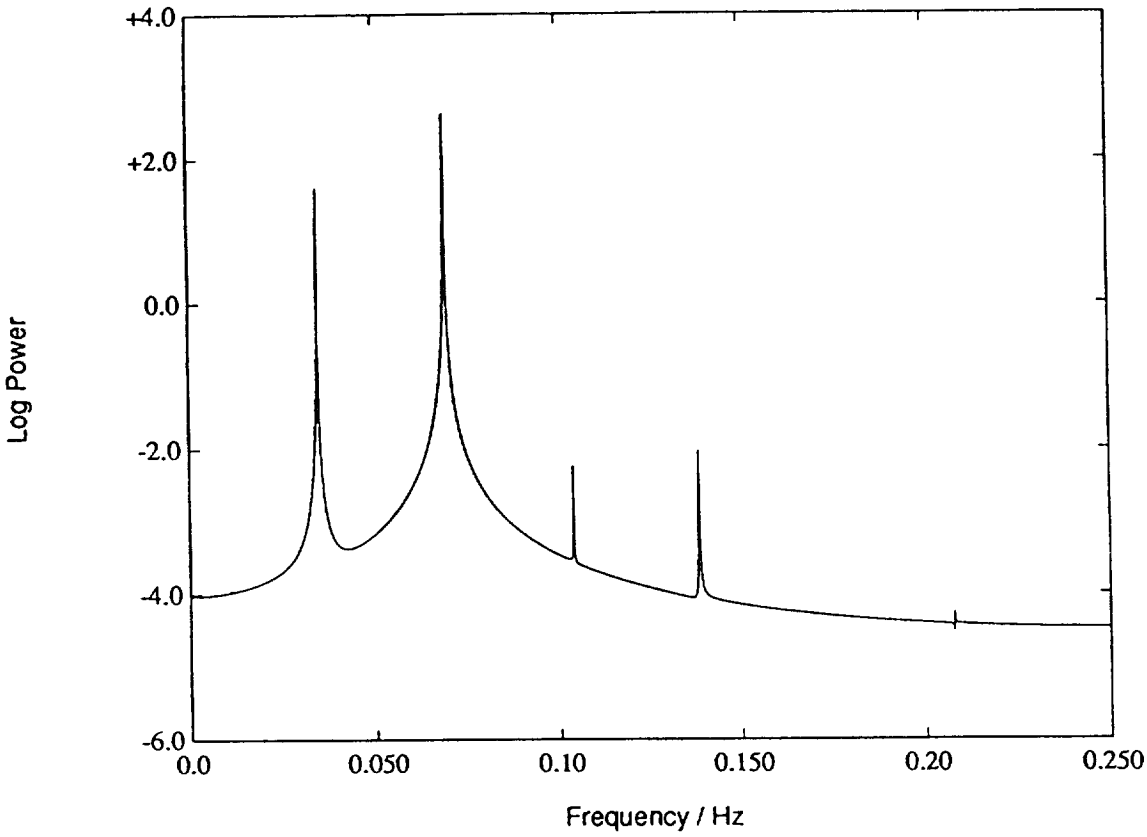

7. Power spectrum of the velocity u at $\Omega = 4\Omega_c$. The principal frequency and its subharmonic dominates the spectrum.

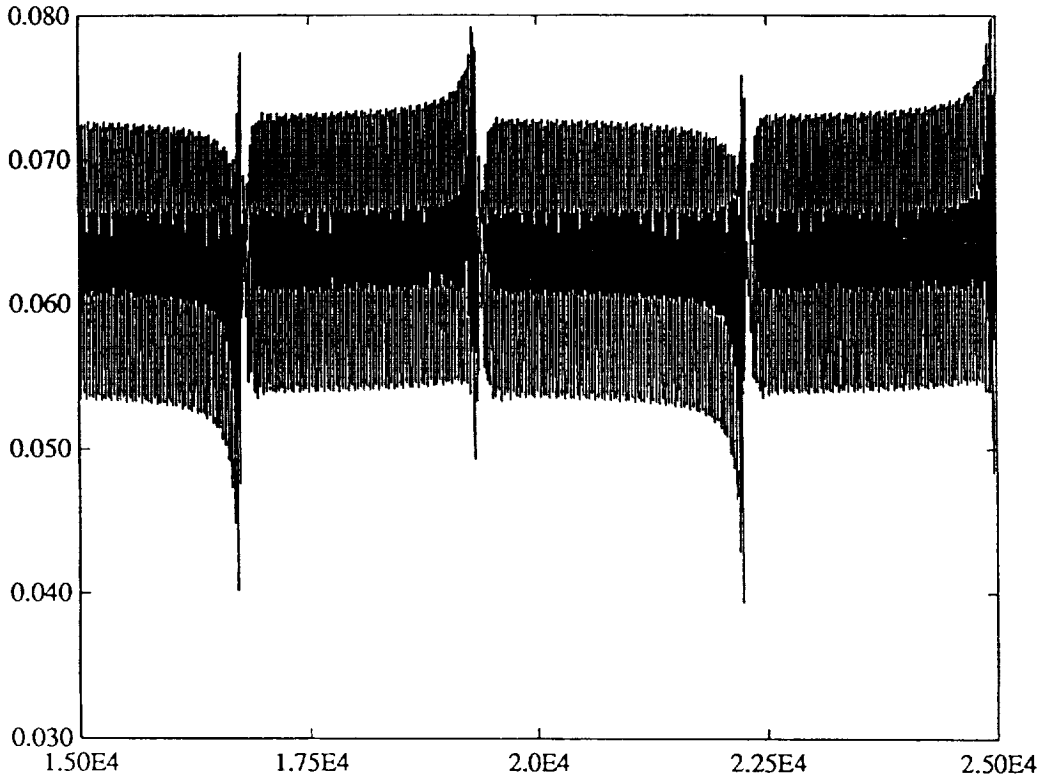

8. a) Time series of $Re(u_{(0,1)})(t)$ at $\Omega = 4.48\Omega_c$. The flow is intermittent chaotic with long time intervals between the bursts of activity.

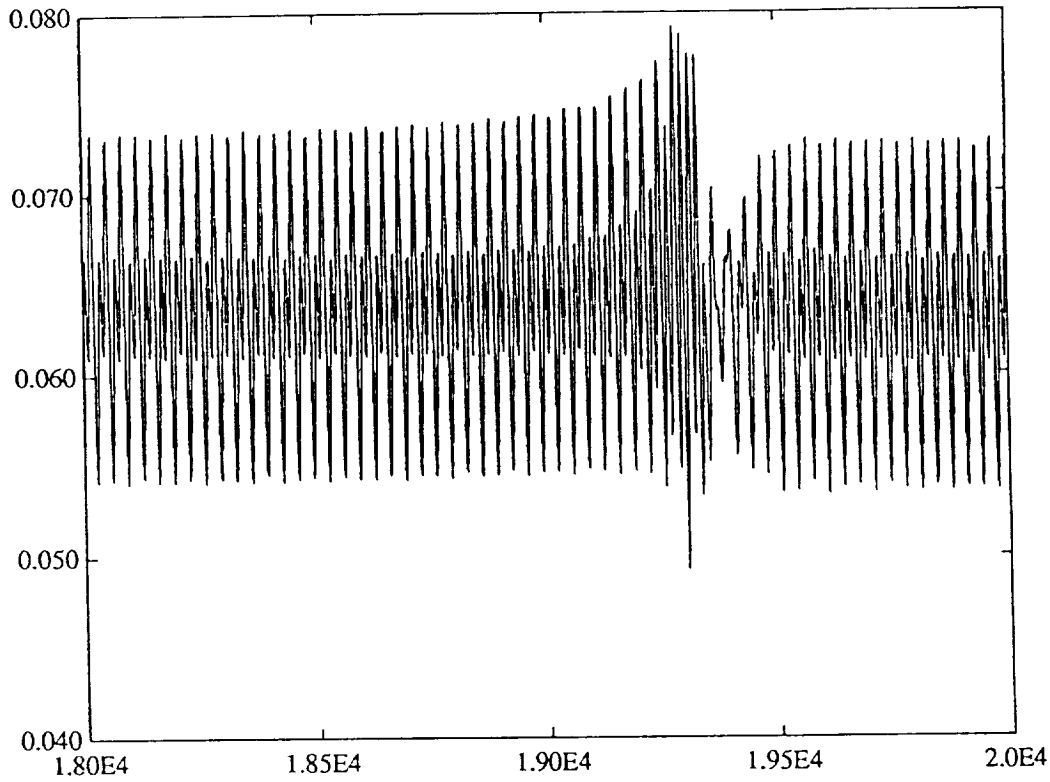

8. b) blow up of a).

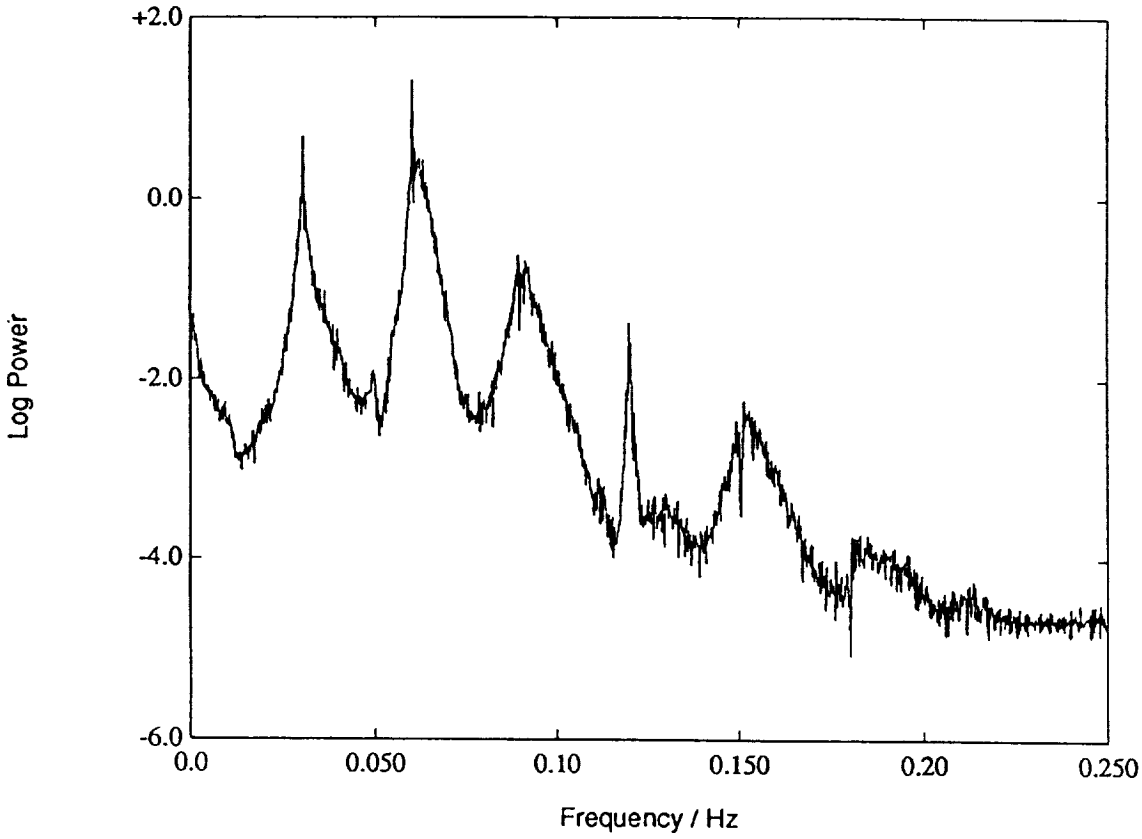

9. Power spectrum of the velocity **u** at $\Omega = 4.48\Omega_c$. The flow is chaotic, but the principal frequency and its subharmonics still dominate the spectrum.

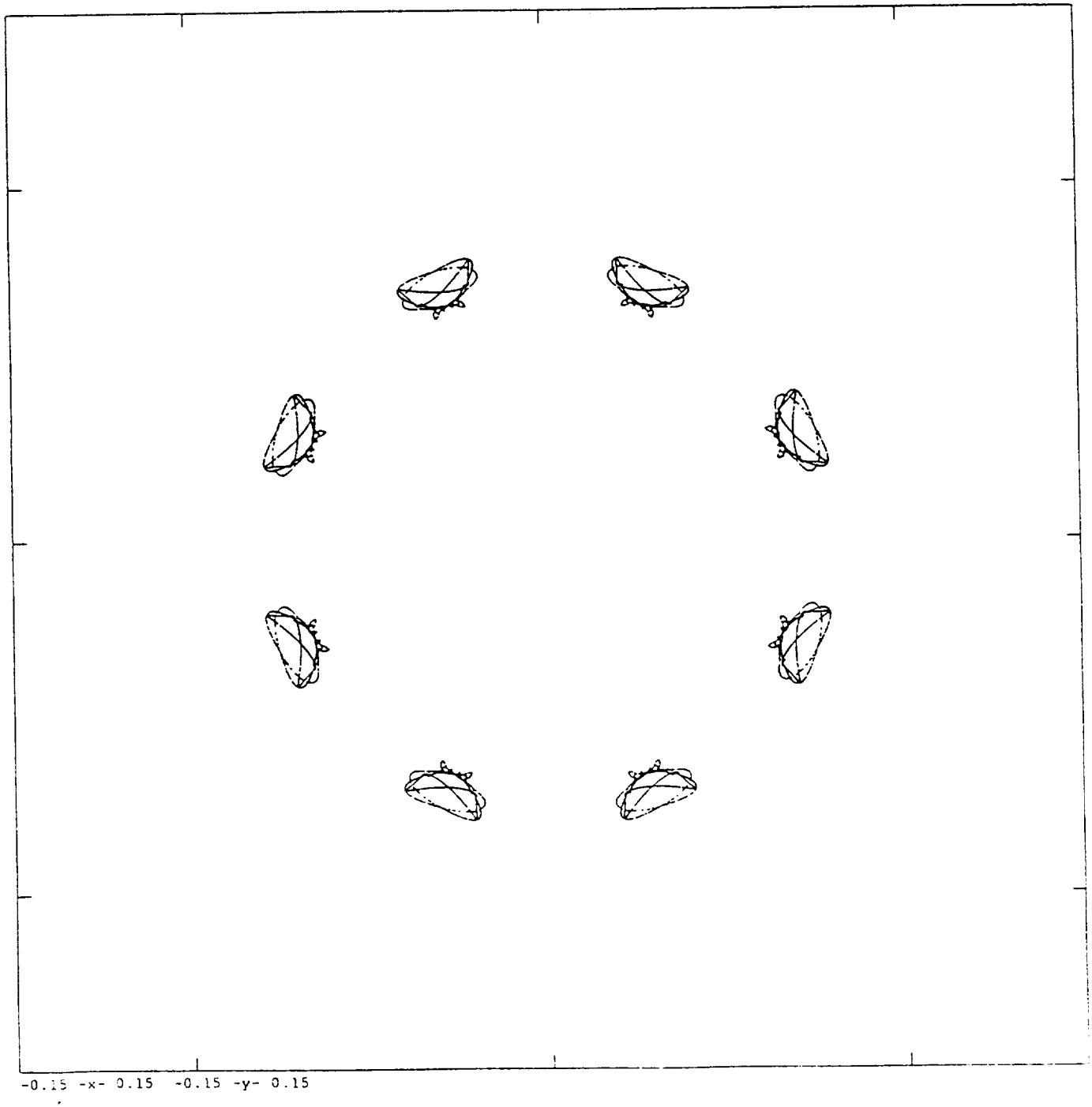

10. a) Poincare section of the chaotic attractors at $\Omega = 4.48\Omega_c$. Attractors are not ergodic.

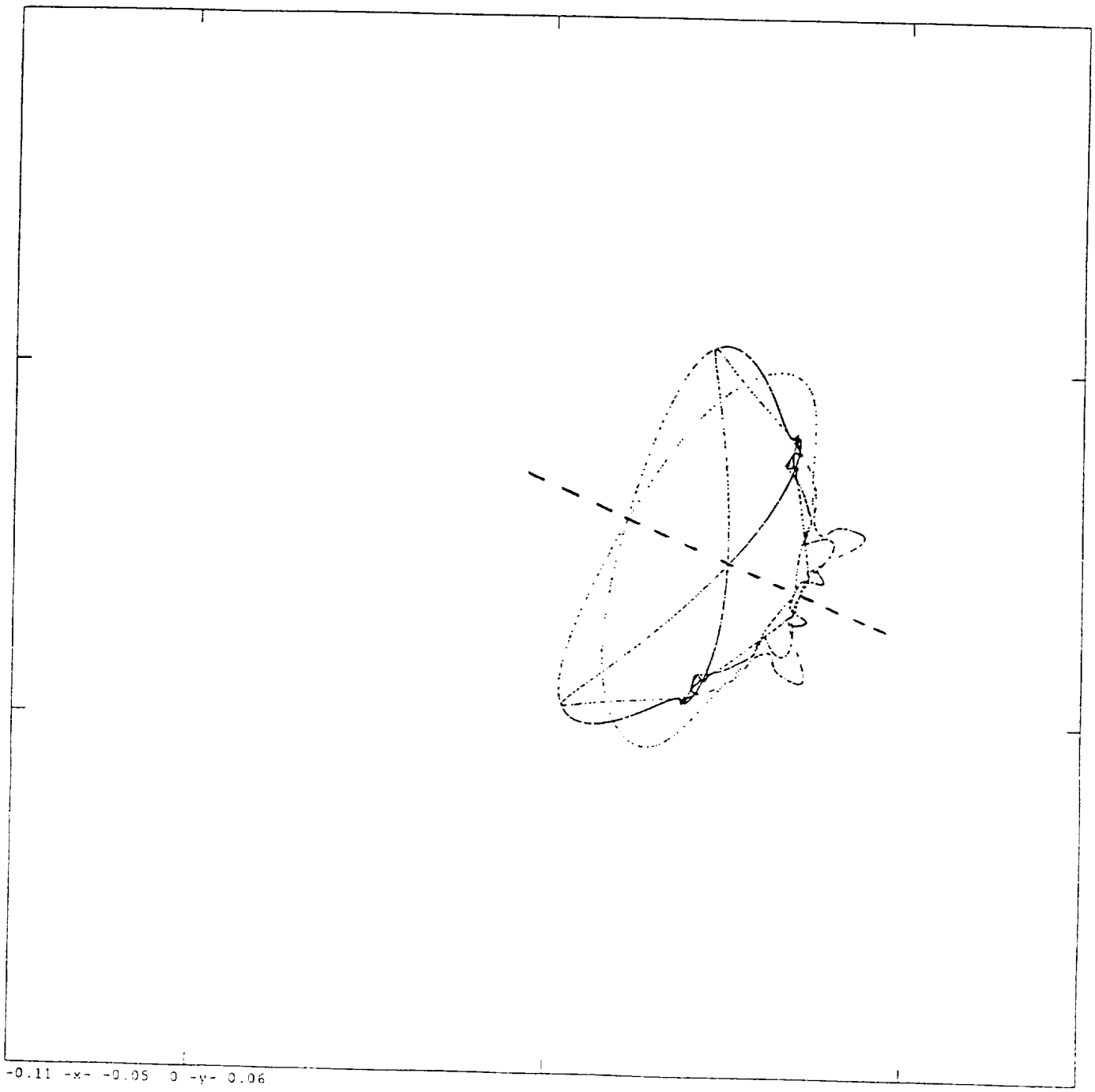

10. b) one of the attractors. Attractors are not ergodic. A dashed line shows axis of symmetry of the attractor.

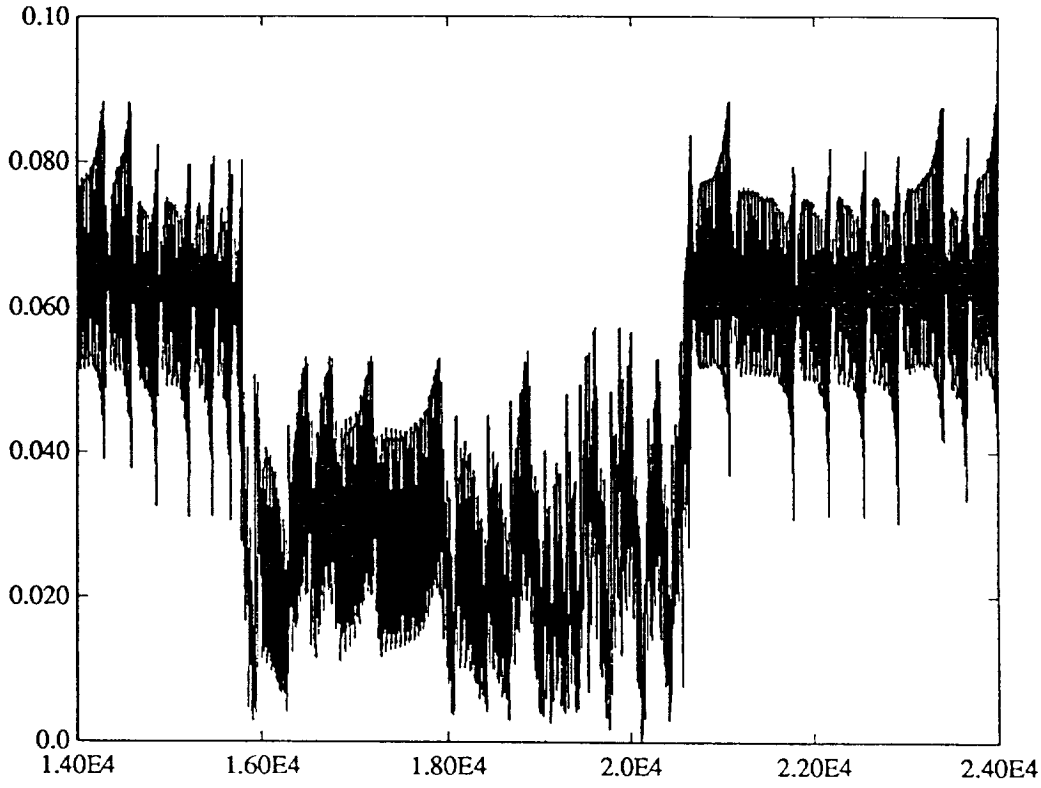

11. a) Time series of $Re(u_{(0,1)})(t)$ at $\Omega = 4.63\Omega_c$. The flow is intermittent chaotic. The sudden jumps correspond to the solution jumping from one component of the chaotic attractor to another.

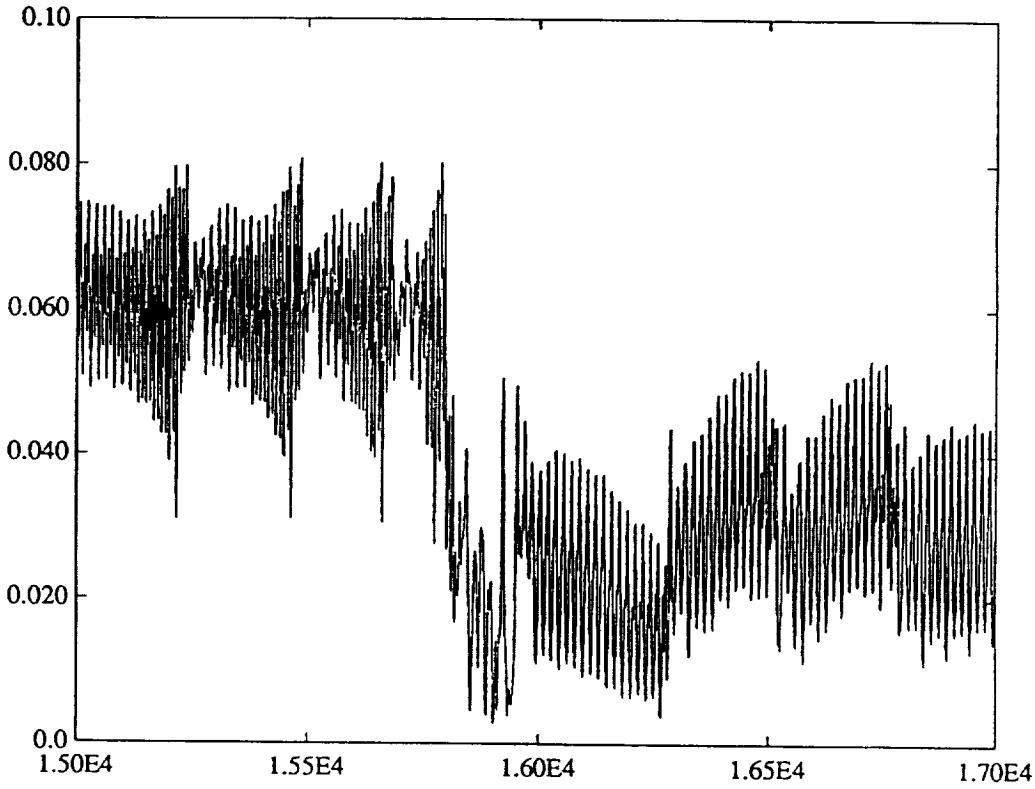

11. b) blow up of a).

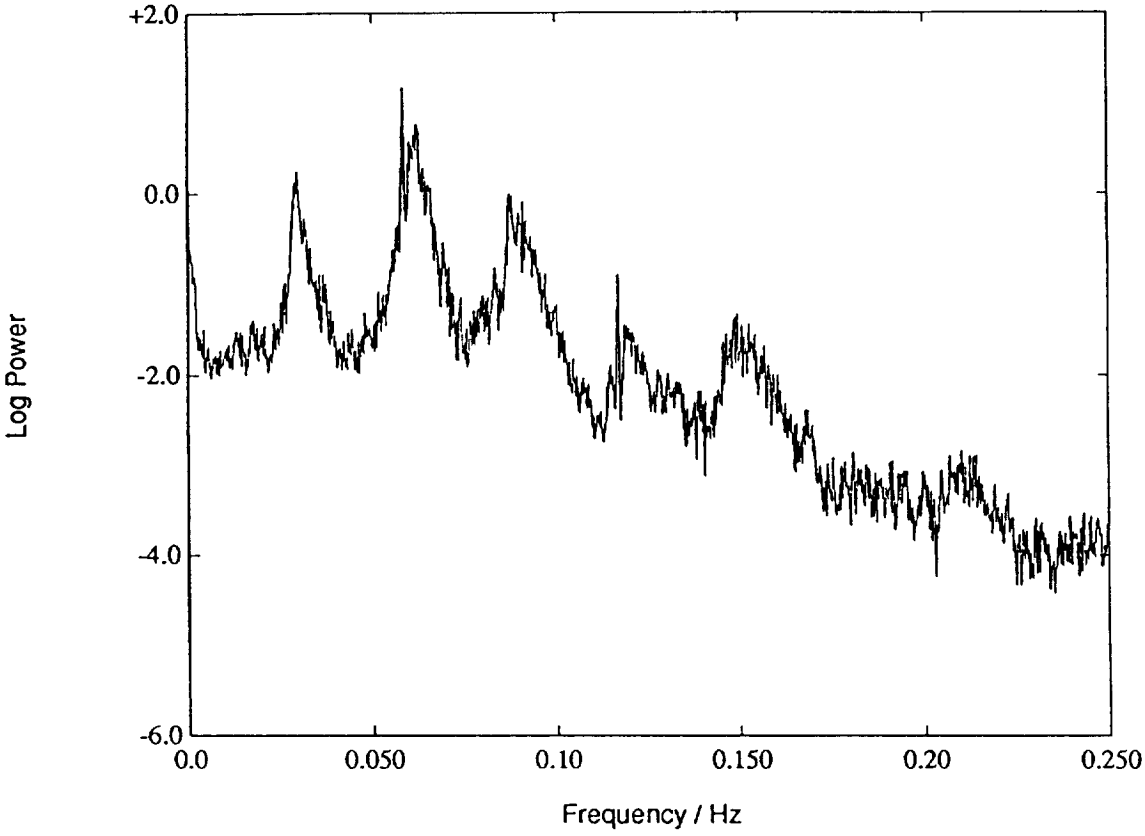

12. Power spectrum of the velocity **u** at $\Omega = 4.63\Omega_c$.

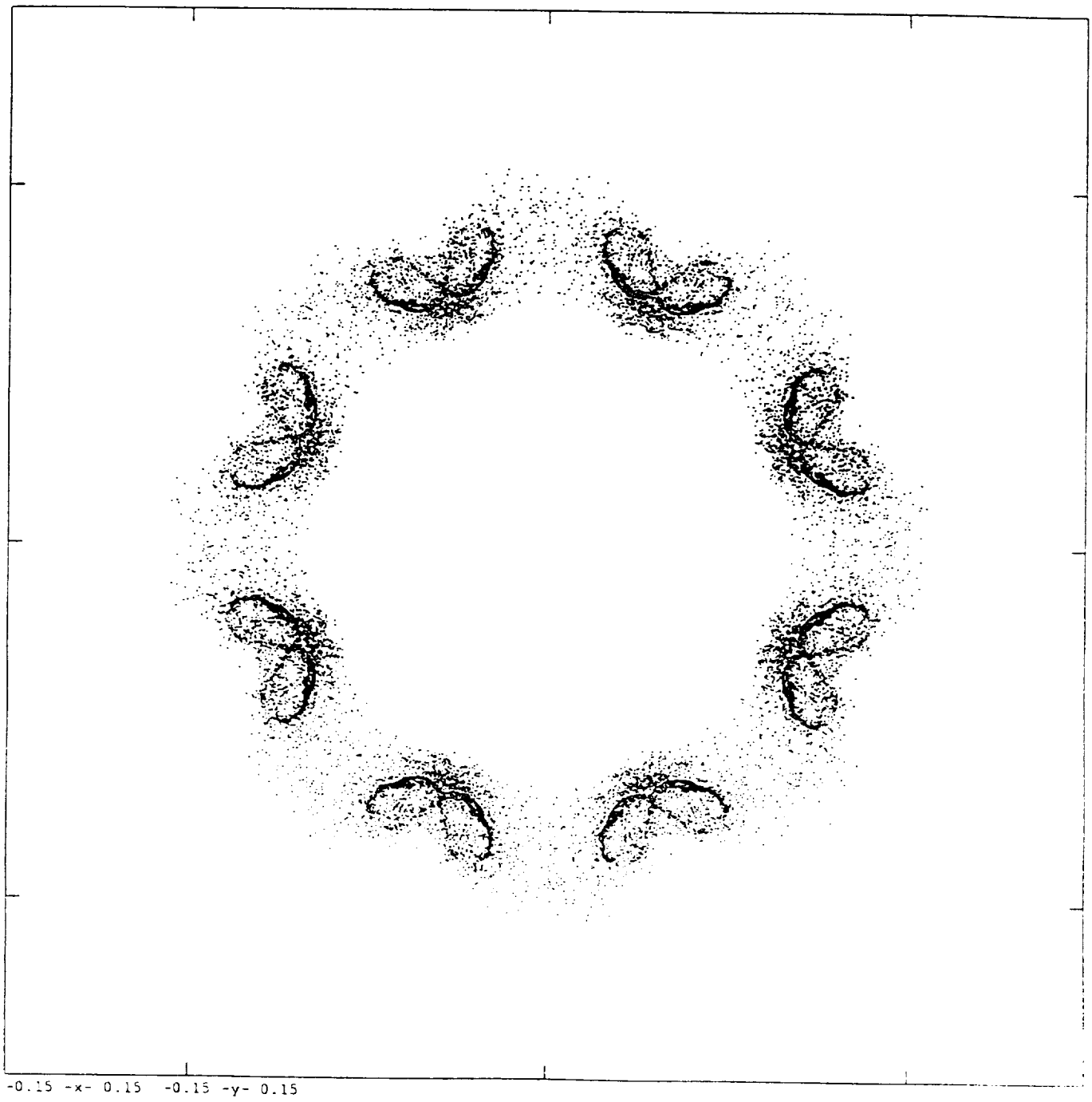

13. a) Poincare section of the chaotic attractor at $\Omega = 4.63\Omega_c$. Flow intermittently jumps from one component of the attractor to another.

13. b) One of the components of the attractor.

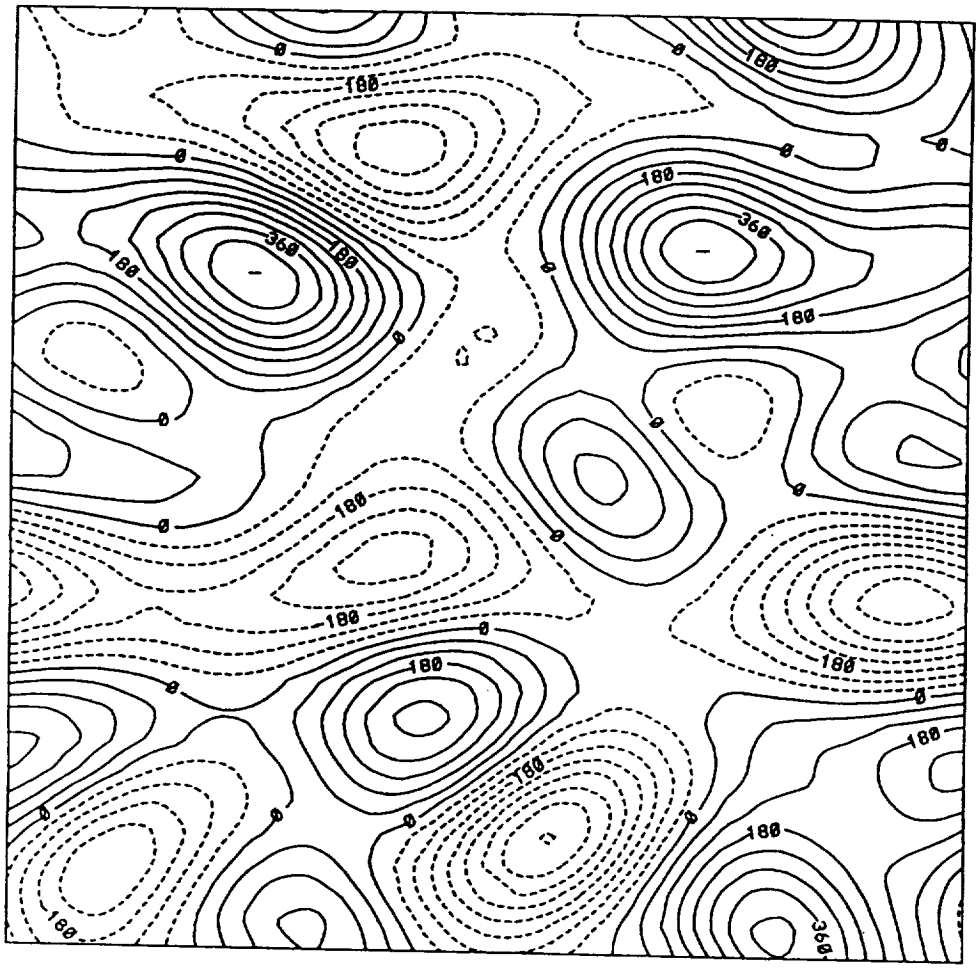

14. Instantaneous flow pattern found in metastable chaotic regime at $\Omega = 10\Omega_c$. a) streamlines. The flow is both spatially and temporally chaotic, and thus may be called turbulent.

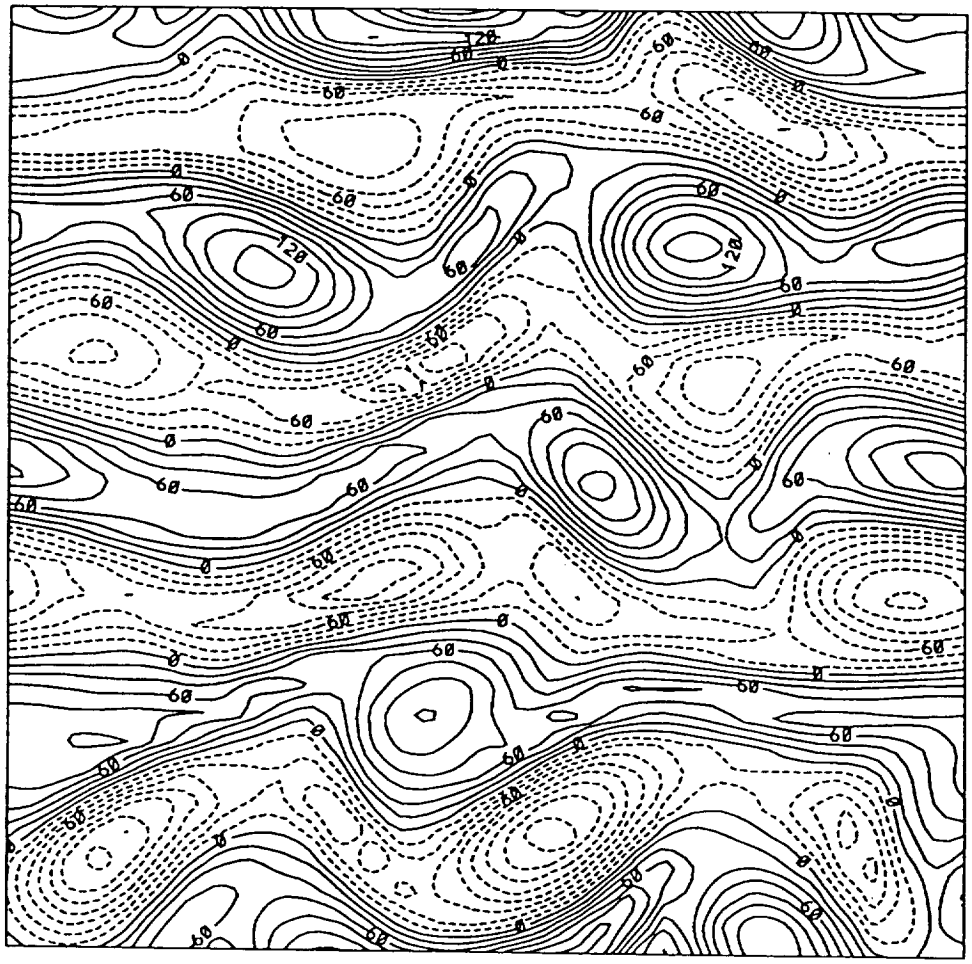

14. Instantaneous flow pattern found in metastable chaotic regime at $\Omega = 10\Omega_c$. b) vorticity. The flow is both spatially and temporally chaotic, and thus may be called turbulent.

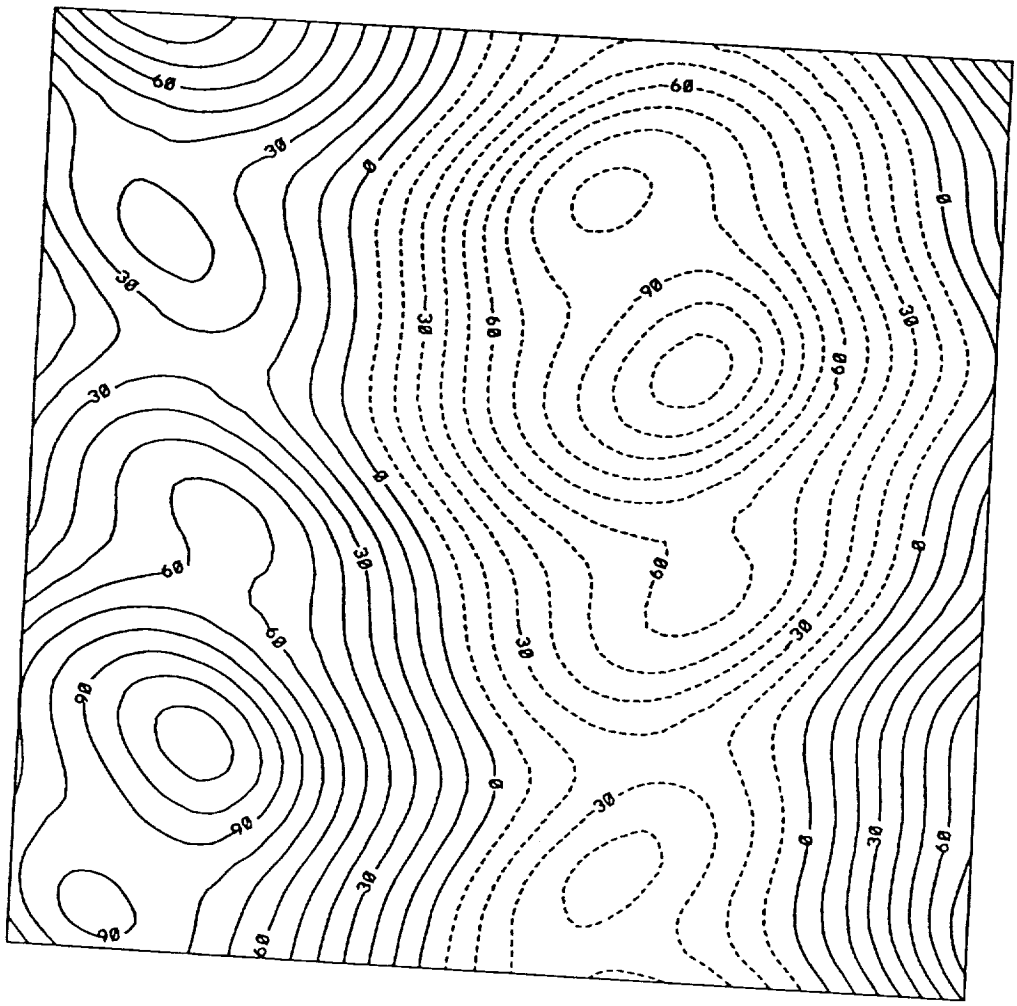

15. Steady spatially chaotic flow found at $\Omega = 5.9\Omega_c$. a) streamlines. Also, this is an example of large scale structures.

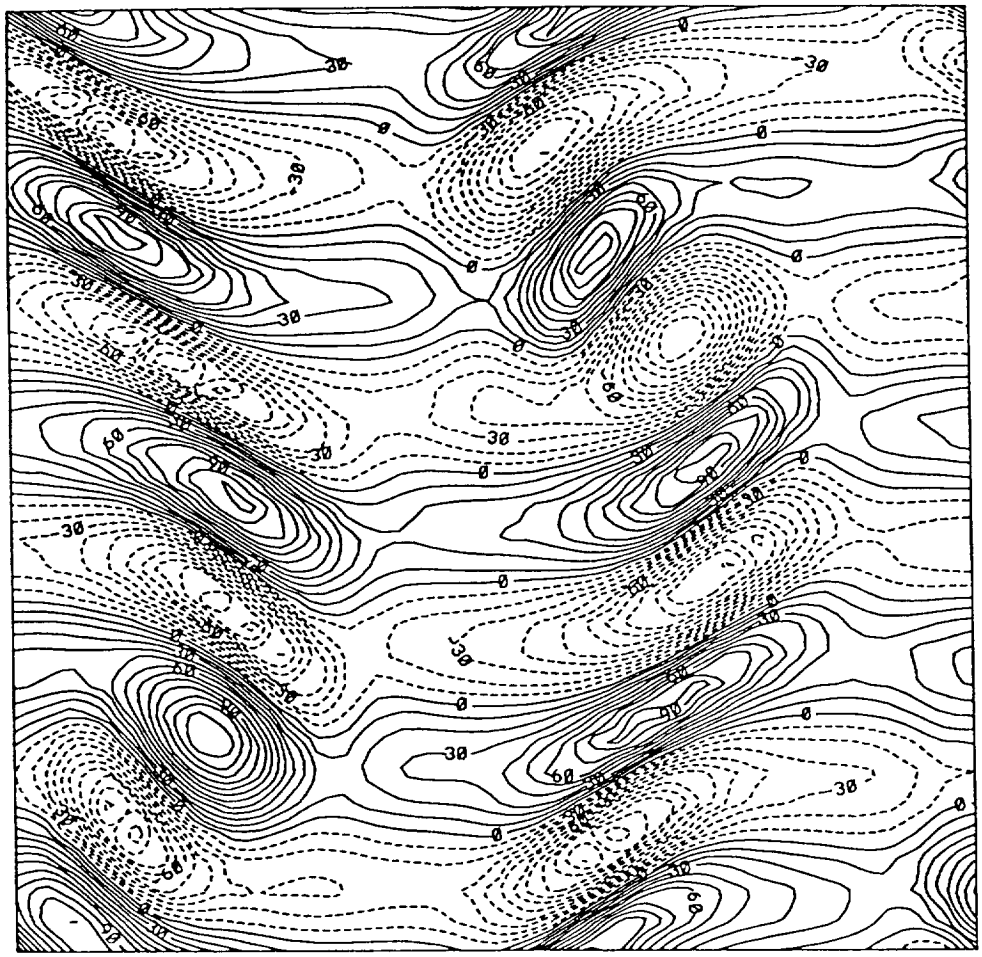

15. Steady spatially chaotic flow found at $\Omega = 5.9\Omega_c$. b) vorticity. Also, this is an example of large scale structures.

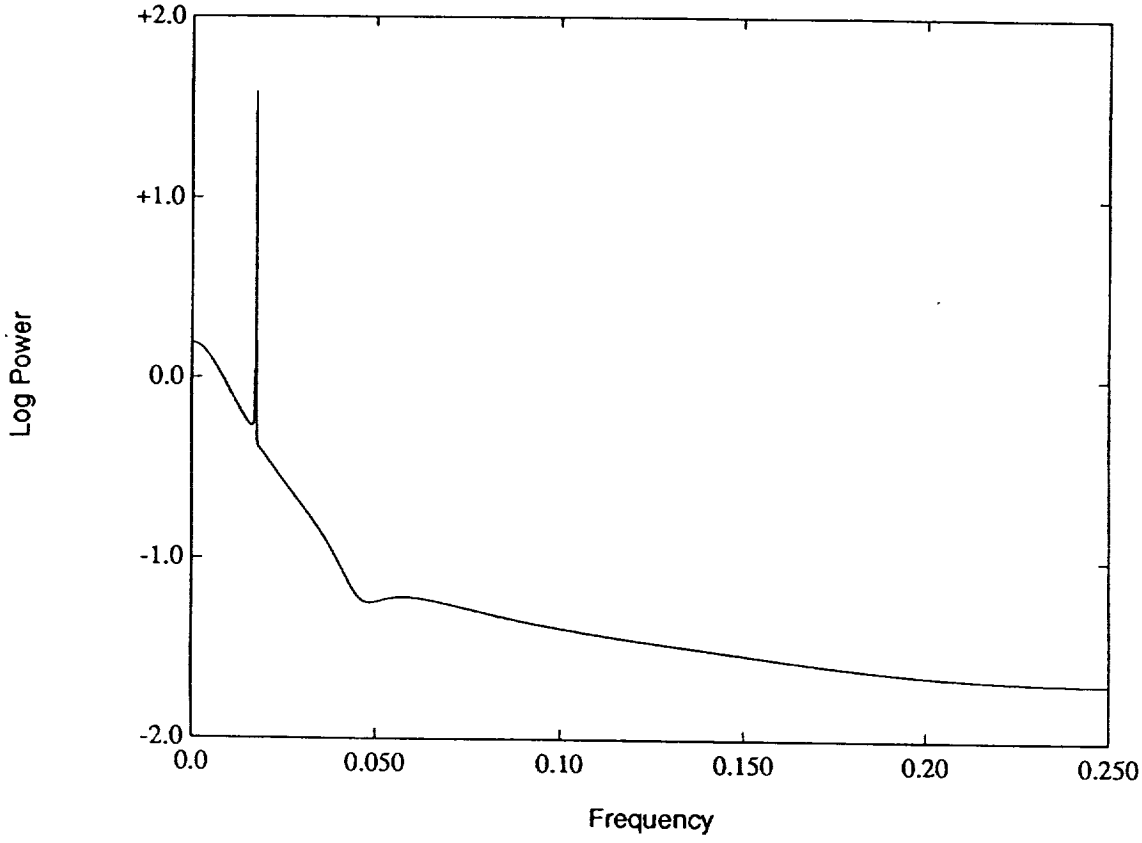

16. Power spectrum of the velocity u at $\Omega = 5\Omega_c$. Only one frequency present in the problem.

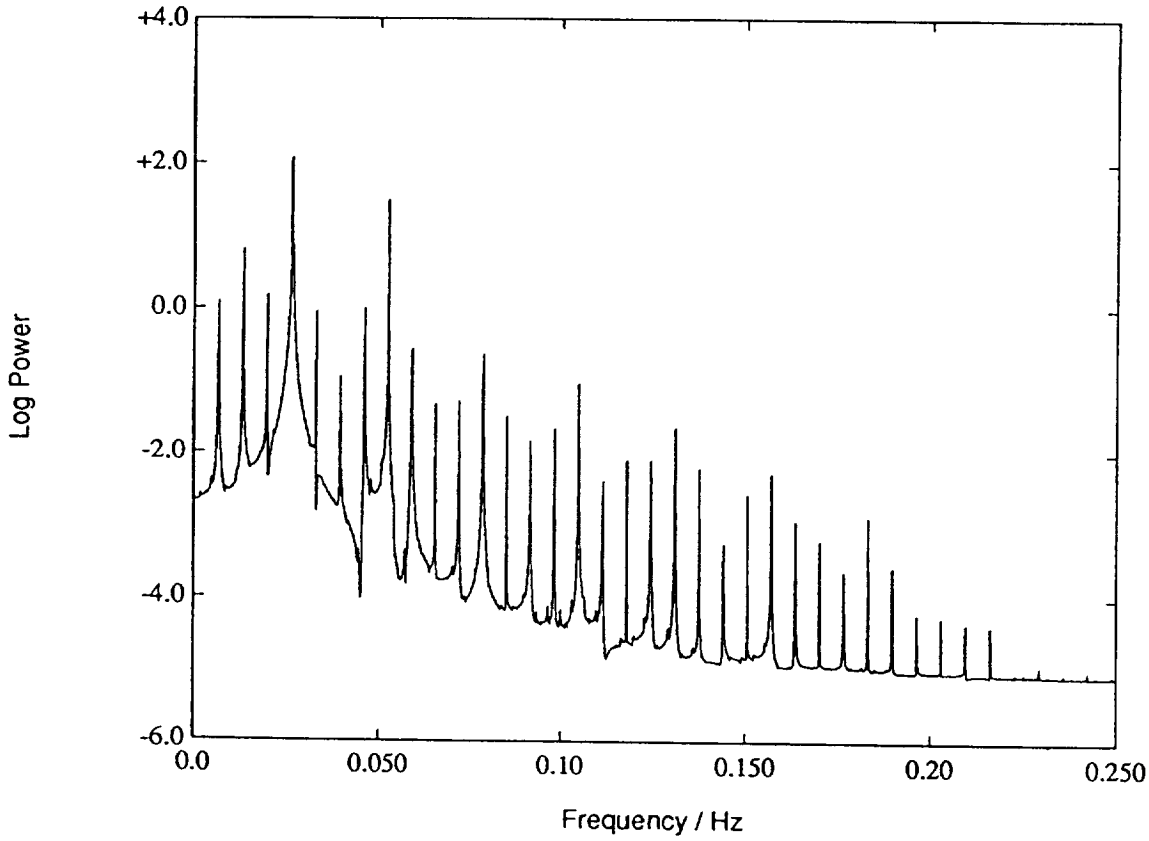

17. Power spectrum of the velocity u at $\Omega = 9.458\Omega_c$. Two period-doublings have taken place.

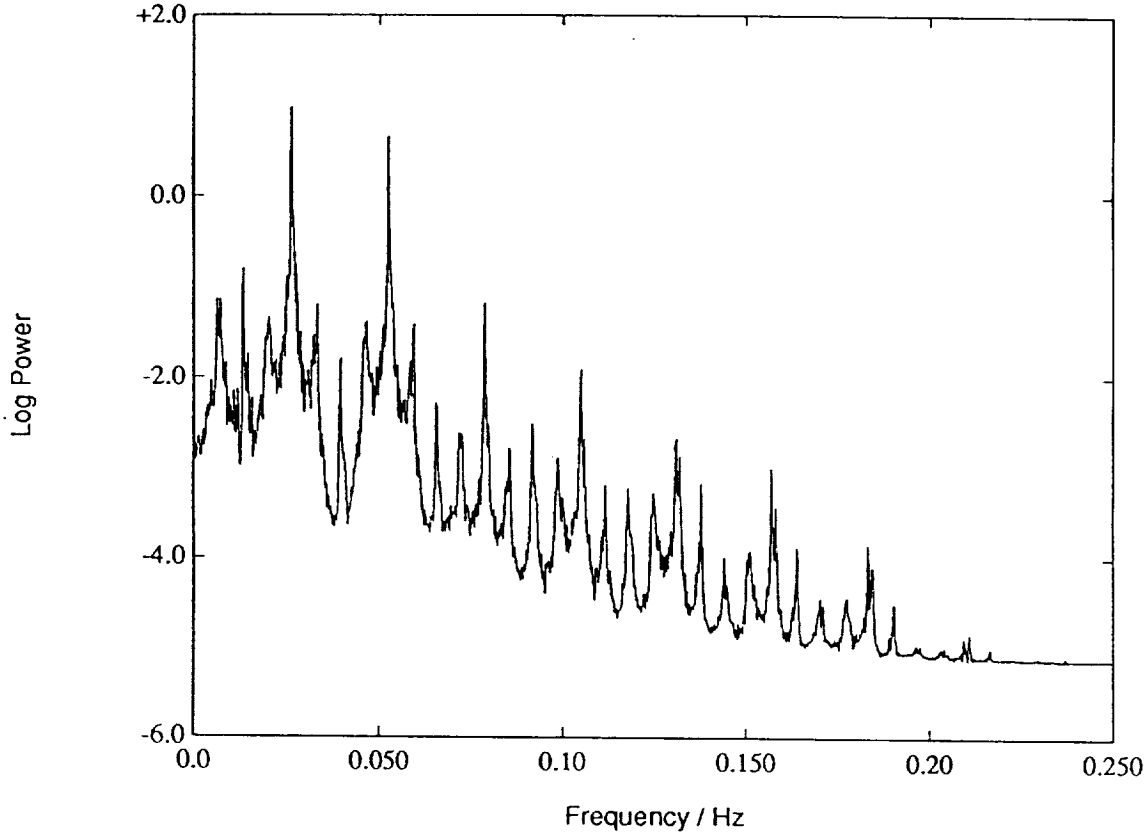

18. Power spectrum of the velocity u at $\Omega = 9.47\Omega_c$. The flow is chaotic, but the driving frequency and its subharmonics are still dominant in the spectrum.

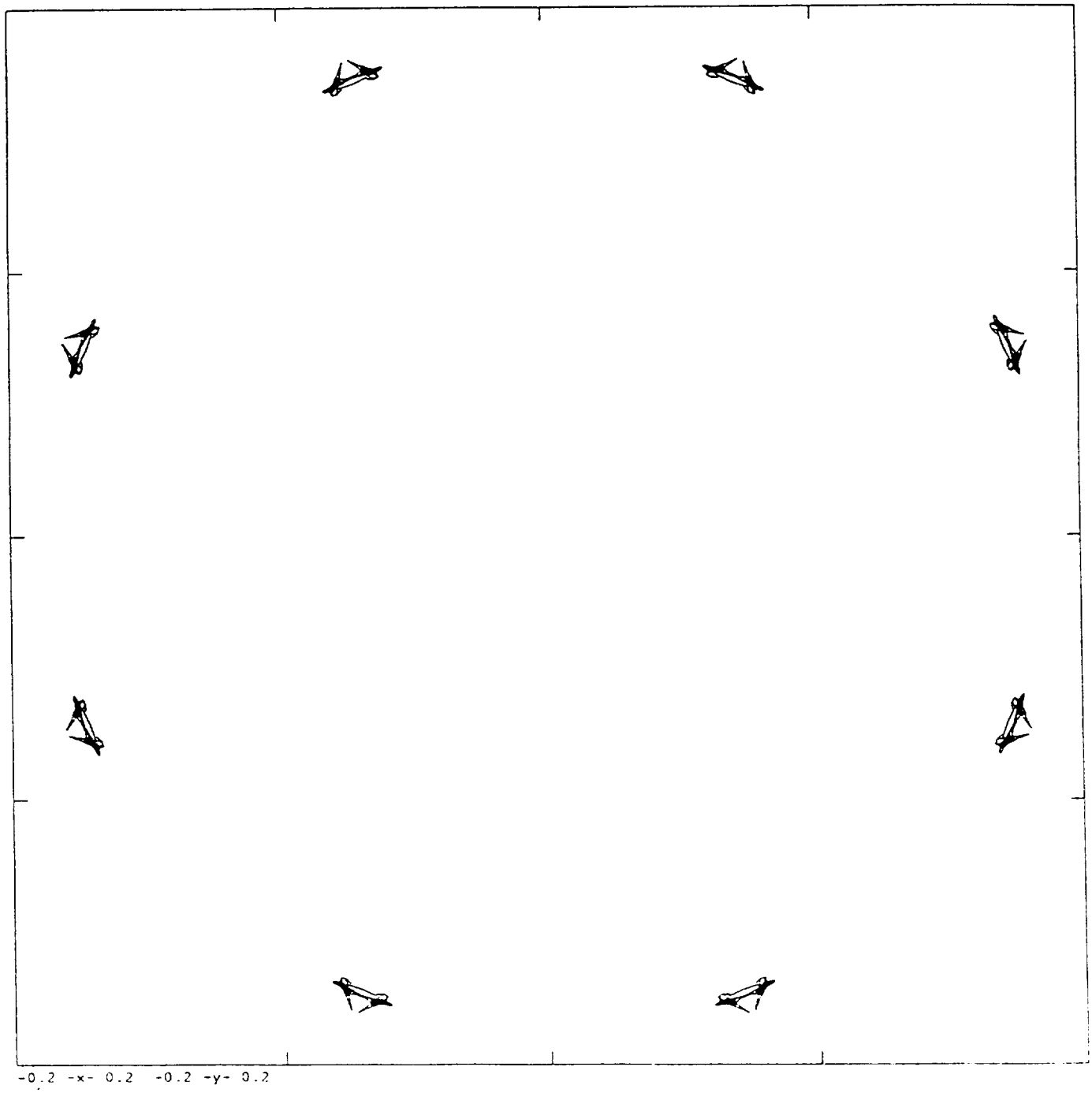

19. a) Poincare sections of the chaotic attractor at $\Omega = 9.47\Omega_c$. Again, attractors are not ergodic.

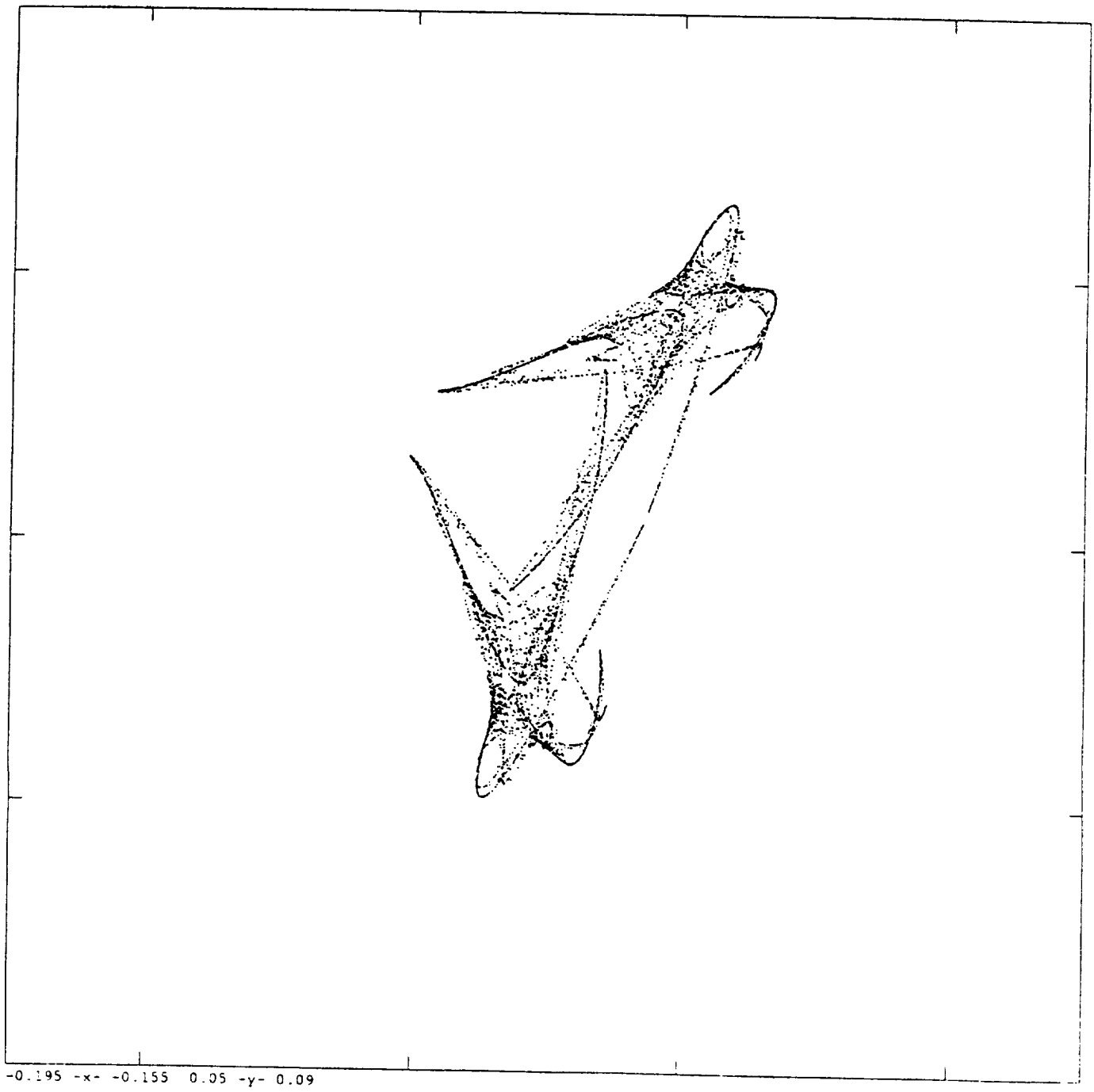

19. b) One of the chaotic attractors.

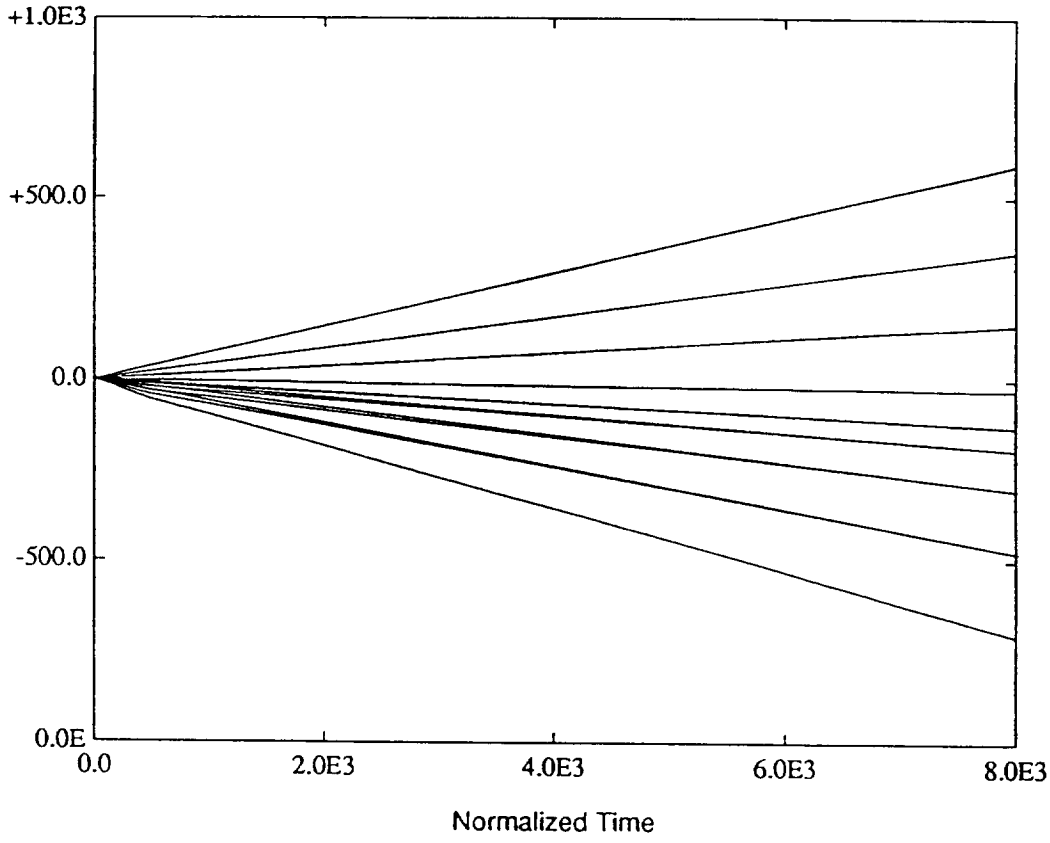

20. Typical curves for the Lyapunov exponents calculations. Here $\Omega = 9.47\Omega_c$ and $d_L = 7.9$.

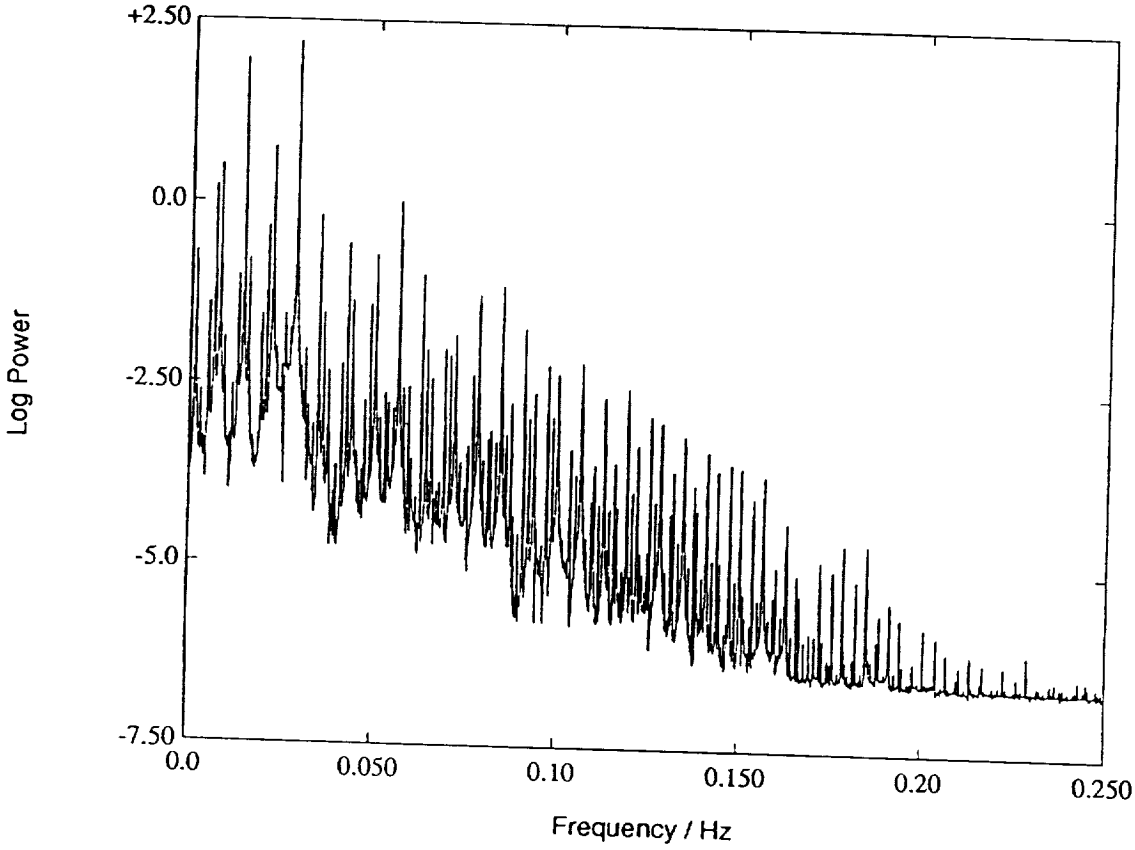

21. Power spectrum of the velocity **u** at $\Omega = 10.7\Omega_c$. One period-doubling have taken place in the range $9.65 \leq \Omega/\Omega_c \leq 10.7$.

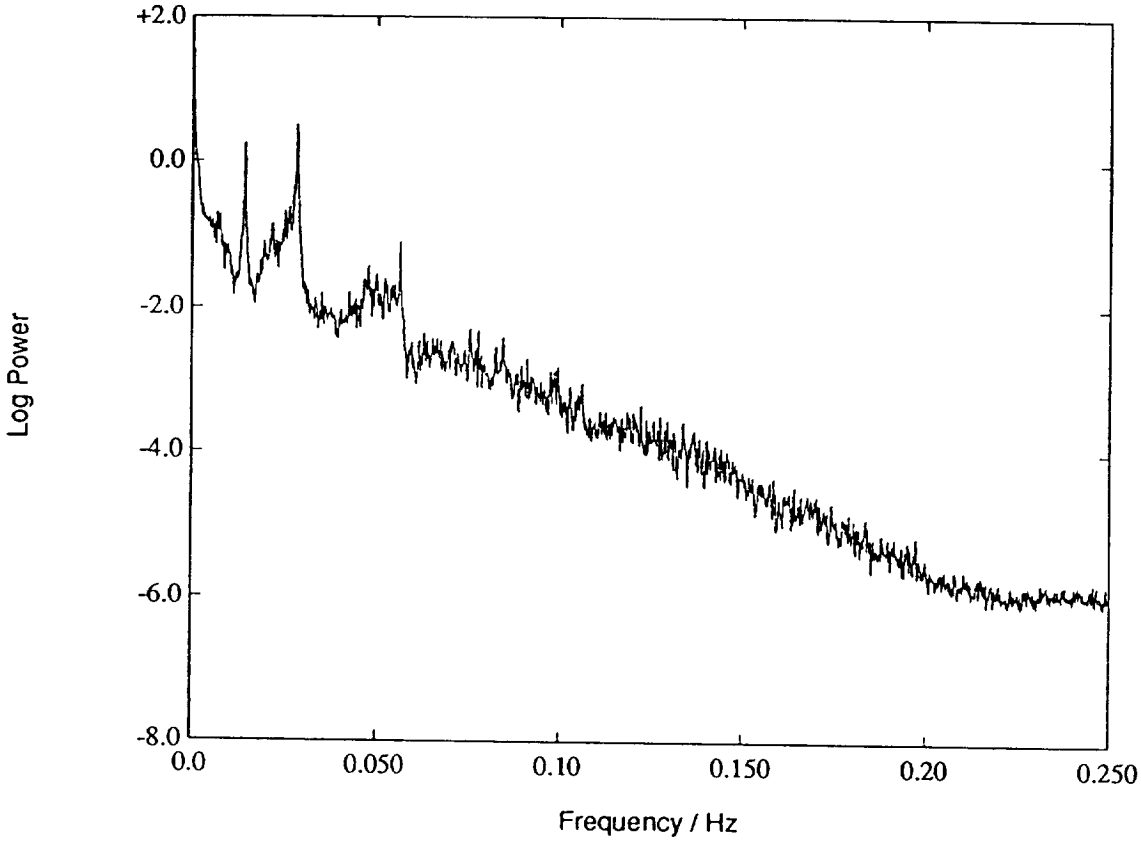

22. Power spectrum of the velocity u at $\Omega = 10.805\Omega_c$. The flow is chaotic, but the driving frequency and its subharmonics are dominant in the spectrum.

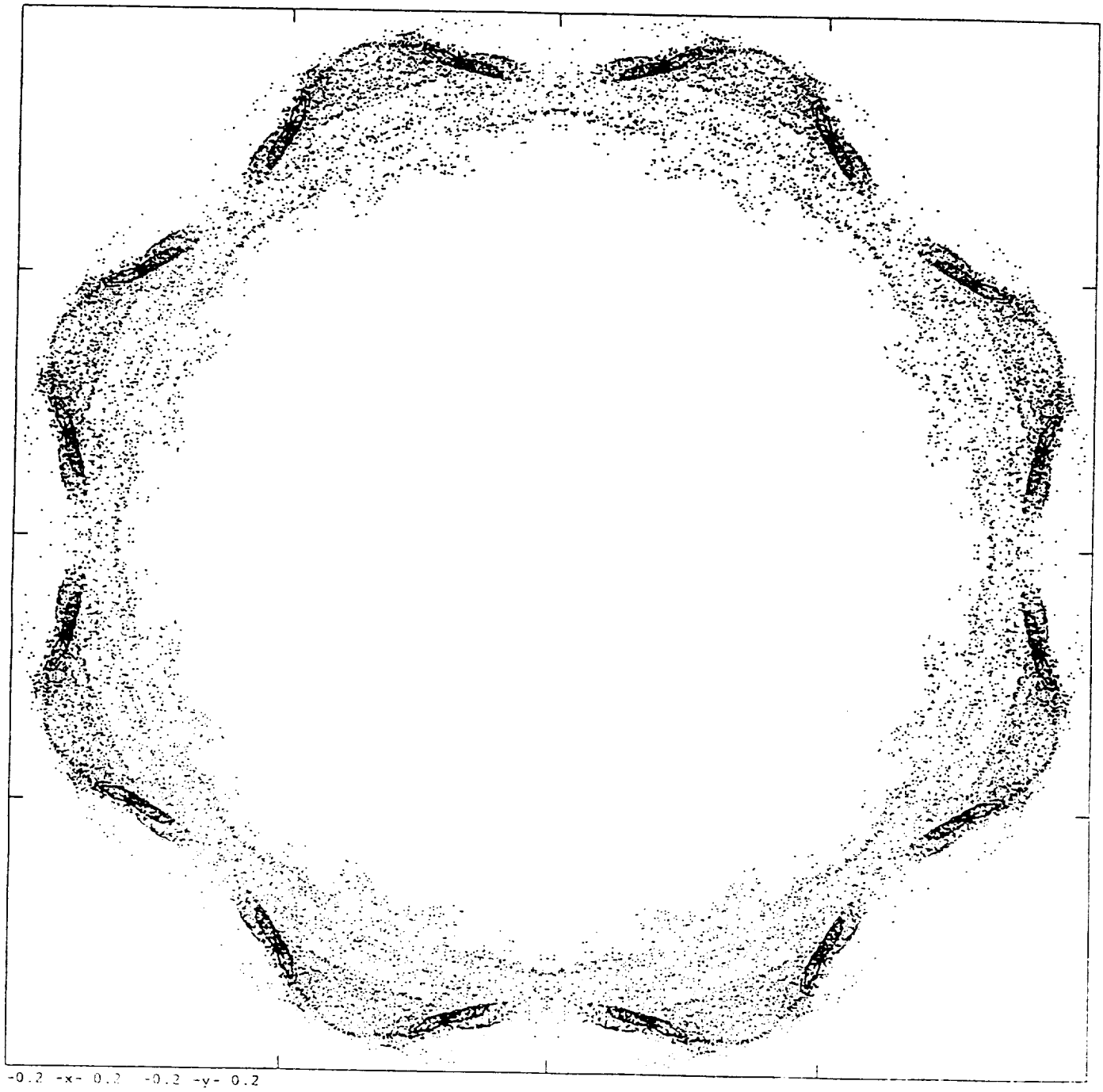

23. a) Poincare section of the chaotic attractor at $\Omega = 10.805\Omega_c$.

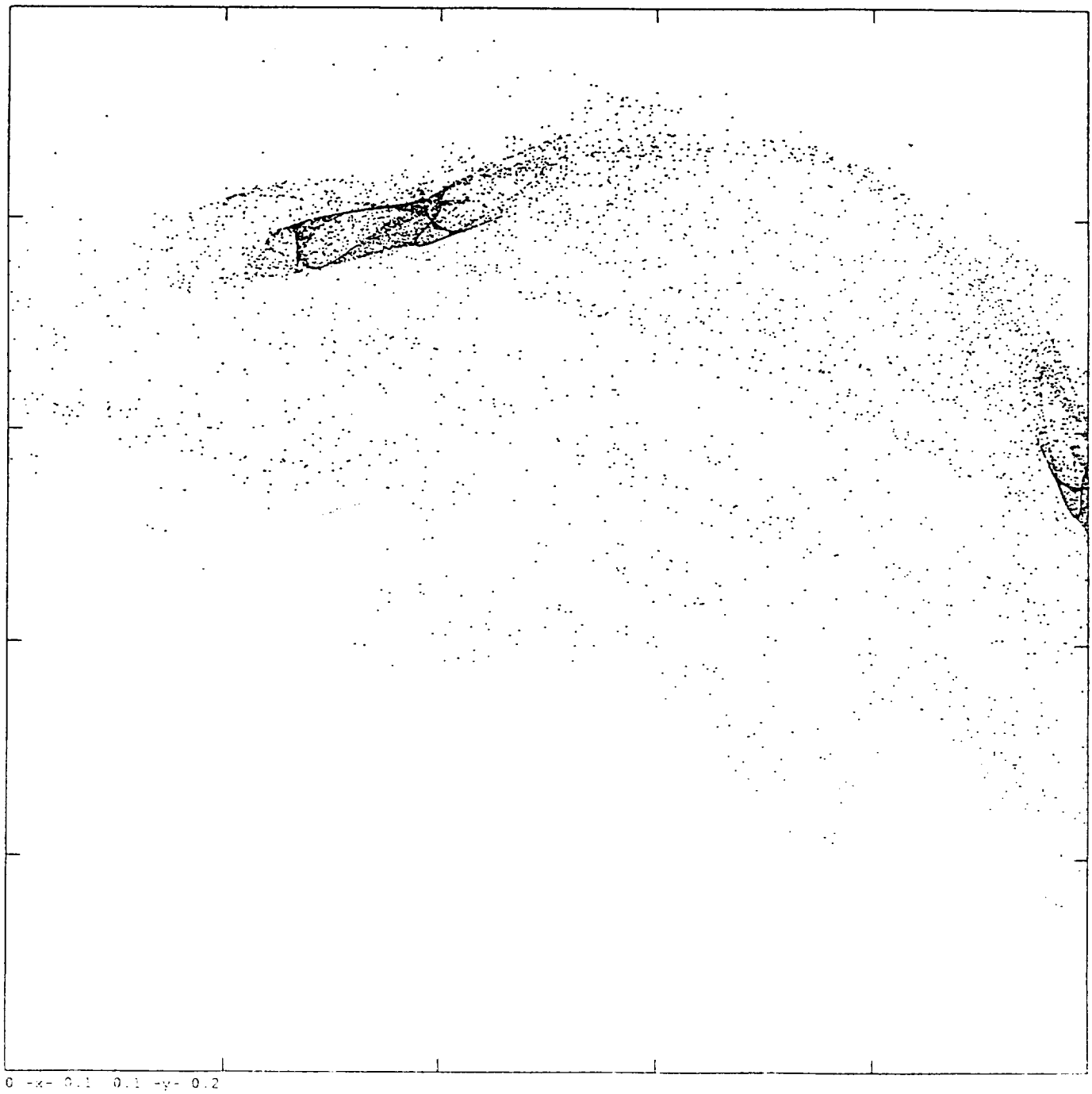

23. b) Blow up of one of the components of the attractor. The fractal structure of the attractor is evident from blow up.

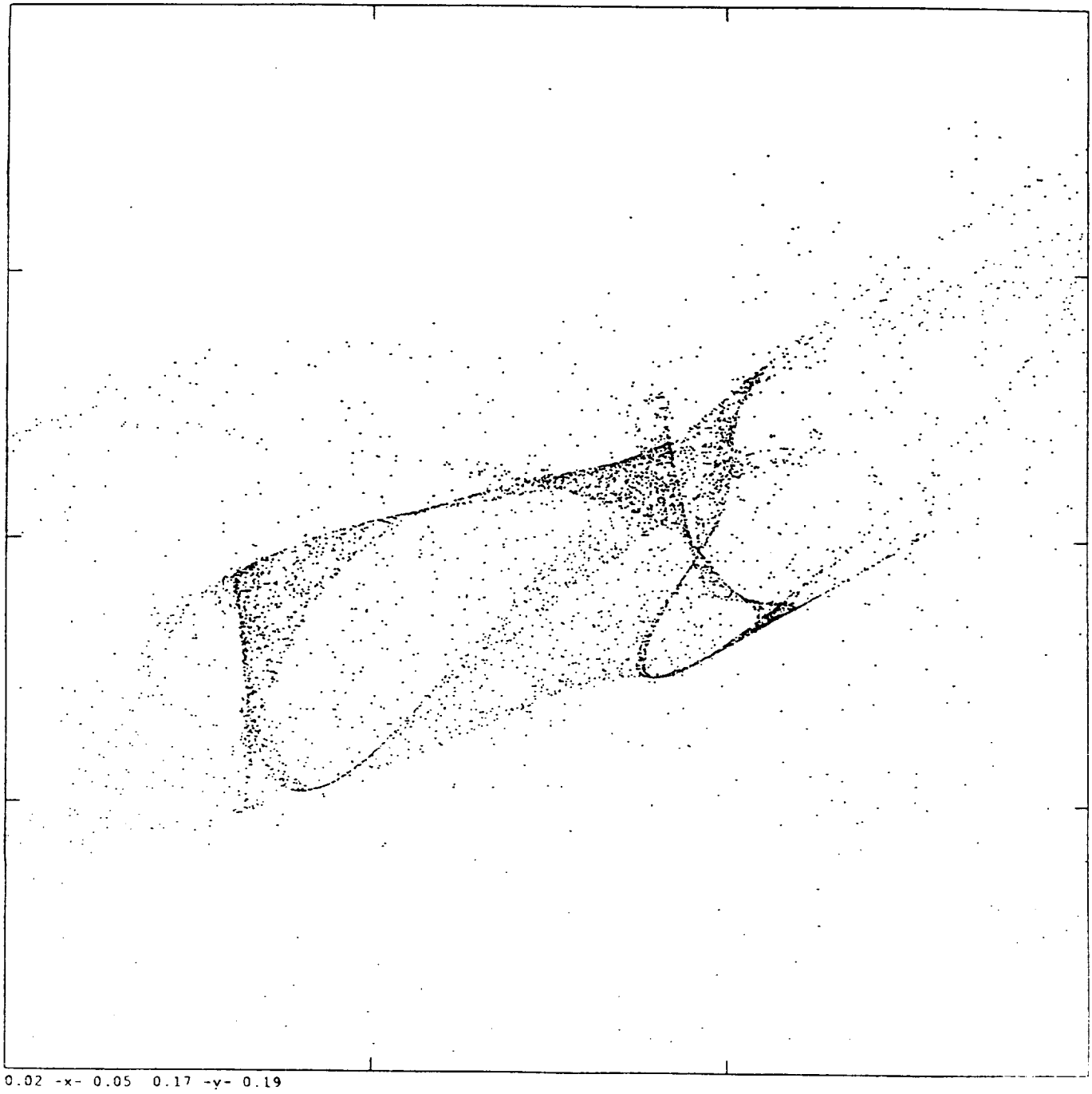

23. c) Blow ups of one of the components of the attractor. The fractal structure of the attractor is evident from blow up.

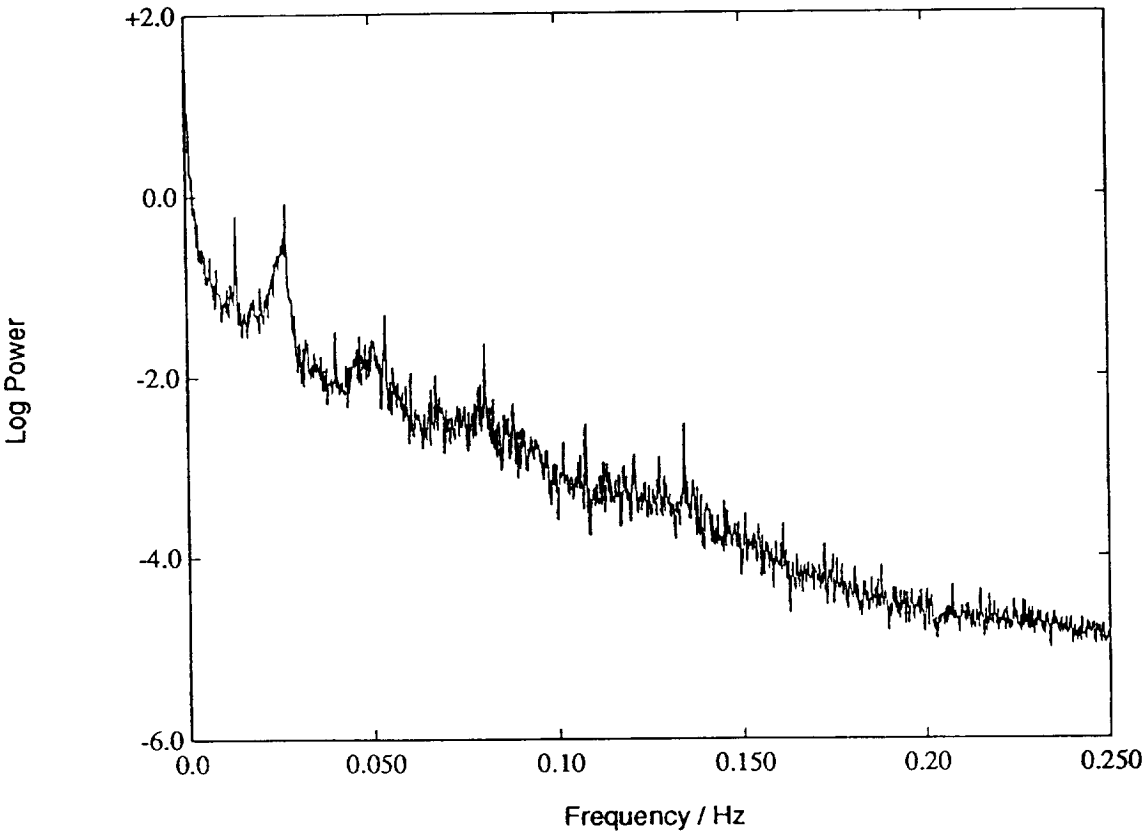

24. Power spectrum of the velocity **u** at $\Omega = 12.5\Omega_c$. The driving frequency and its subharmonics are still dominant in the spectrum.

NASA
National Aeronautics and Space Administration

Report Documentation Page

1. Report No.	2. Government Accession No.	3. Recipient's Catalog No.
NASA CR-182079 ICASE Report No. 90-50		

4. Title and Subtitle	5. Report Date
AN INVESTIGATION OF CHAOTIC KOLMOGOROV FLOWS	August 1990
	6. Performing Organization Code

7. Author(s)	8. Performing Organization Report No.
N. Platt L. Sirovich N. Fitzmaurice	90-50
	10. Work Unit No. 505-90-21-01

9. Performing Organization Name and Address	11. Contract or Grant No.
Institute for Computer Applications in Science and Engineering Mail Stop 132C, NASA Langley Research Center Hampton, VA 23665-5225	NAS1-18605
	13. Type of Report and Period Covered Contractor Report

12. Sponsoring Agency Name and Address	14. Sponsoring Agency Code
National Aeronautics and Space Administration Langley Research Center Hampton, VA 23665-5225	

15. Supplementary Notes

Langley Technical Monitor:
Richard W. Barnwell

Submitted to Physics of Fluids

Final Report

16. Abstract

A two-dimensional flow governed by the incompressible Navier-Stokes equations with a steady spatially periodic forcing (known as the Kolmogorov flow) is numerically simulated. The behavior of the flow and its transition states as the Reynolds number **Re** varies is investigated in detail, as well as a number of the flow feaures. A sequence of bifurcations is shown to take place in the flow as **Re** varied. Two main regimes of the flow have been observed: small and large scale structure regimes corresponding to different ranges of **Re**. Each of the regimes includes a number of quasiperiodic, chaotic and relaminarization windows. In addition, each range contains a chaotic window with non-ergodic chaotic attractors. Spatially disordered, but temporally steady states have been discovered in large scale structure regime. Features of the diverse cases are displayed in terms of the temporal power spectrum, Poincare sections and, where possible, Lyapunov exponents and Kaplan-Yorke dimension.

17. Key Words (Suggested by Author(s))	18. Distribution Statement
coherence structures, 2-dimensional turbulence, chaos	34 - Numerical Analysis and Heat Transfer Unclassified - Unlimited

19. Security Classif. (of this report)	20. Security Classif. (of this page)	21. No. of pages	22. Price
Unclassified	Unclassified	77	A05